GEOLOGICA CARPATHICA, APRIL 2020, 71, 2, 166–182 https://doi.org/10.31577/GeolCarp.71.2.5

$^{40}Ar/^{39}Ar$ geochronology using high sensitivity mass spectrometry: Examples from middle Miocene horizons of the Central Paratethys

KARIN SANT[1], KLAUDIA F. KUIPER[2], SAMUEL RYBÁR[3,✉],PATRICK GRUNERT[4], MATHIAS HARZHAUSER[5], OLEG MANDIC[5],MICHAL JAMRICH[3], KATARÍNA ŠARINOVÁ[6], NATÁLIA HUDÁČKOVÁ[3] and WOUT KRIJGSMAN[1]

[1]Paleomagnetic Laboratory 'Fort Hoofddijk', Utrecht University, Budapestlaan 17, 3584 CD Utrecht, The Netherlands; karin.sant@gmail.com, w.krijgsman@uu.nl
[2]Vrije Universiteit Amsterdam, Department of Earth Sciences, Faculty of Science, De Boelelaan 1085, 1081HV Amsterdam, The Netherlands; k.f.kuiper@vu.nl
[3]Department of Geology and Paleontology, Faculty of Natural Sciences, Comenius University in Bratislava, Mlynská dolina, Ilkovičova 6, 842 15 Bratislava, Slovakia; ✉samuelrybar3@gmail.com, mjamrich@gmail.com, natalia.hudackova@uniba.sk
[4]Institute of Geology and Mineralogy, University of Cologne, Zülpicher Strasse 49a, 50674 Cologne, Germany; pgrunert@uni-koeln.de
[5]Geological–Paleontological Department, Natural History Museum Vienna, Burgring 7, 1010 Wien, Austria; mathias.harzhauser@nhm-wien.ac.at, oleg.mandic@nhm-wien.ac.at
[6]Department of Mineralogy and Petrology, Faculty of Natural Sciences, Comenius University in Bratislava, Mlynská dolina, Ilkovičova 6, 842 15 Bratislava, Slovakia; katarina.sarinova@uniba.sk

(Manuscript received July 31, 2018; accepted in revised form January 29, 2020; Associated Editor: Jaroslav Lexa)

Abstract: $^{40}Ar/^{39}Ar$ radio-isotopic dating of volcanic tuffs intercalated in sediments can provide high accuracy age control on the deposition of sedimentary rocks. State-of-the-art mass spectrometers such as the ARGUS VI+ are able to acquire highly precise ages for relatively small single grains (~90–250 μm for Miocene samples). Single grain measurement can provide insight into the sometimes complex age distributions within volcanic tuffs. The results show that $^{40}Ar/^{39}Ar$ ages based on multiple grain fusions will not necessarily reflect eruption ages, which can lead to (slight) overestimation of the depositional age. The paper compares multiple and single grain data from different Miocene tuffs in the Central Paratethys, which plays an important role in the establishment of a geological time frame for this area. The examples come from three middle Miocene tuff horizons that span from the Badenian transgression to the Badenian–Sarmatian Extinction Event. The new ages obtained from the Quellgraben section in the Styrian Basin (14.31±0.27 Ma and 14.03±0.04 Ma) are much younger than the previous dating and together with the new data from the Bernhardsthal-4 well, Vienna Basin (15.12±0.19 Ma) indicate, that the Badenian (Langhian) marine flooding did not reach this area before 15.2 Ma. The new weighted mean age of 12.56±0.10 Ma from the Kamenica nad Hronom section in the Danube Basin dates the transition from marine to terrestrial setting, which is possibly connected with a sea level lowstand at the beginning of the Sarmatian.

Keywords: $^{40}Ar/^{39}Ar$ geochronology, Badenian, Styrian Basin, Vienna Basin, Danube Basin.

Introduction

Radio-isotopic $^{40}Ar/^{39}Ar$ dating can provide high quality age control on stratigraphic records. The most recent state-of-the-art mass spectrometers, such as the improved ARGUS VI+, are now able to acquire excellent dating results from single grain measurements on relatively small grains (~90–250 μm). The single grain measurements also provide detailed insight into the age distribution within a tuff sample. By utilizing this asset, it is possible to compare multiple and single grain data from the same samples. In addition, it is possible to re-evaluate the results of previously published $^{40}Ar/^{39}Ar$ ages that were obtained by previous generation conventional mass spectrometers. The reliability of $^{40}Ar/^{39}Ar$ ages can, however, only be judged when laboratory procedures and data interpretation, supported by statistical analyses, are properly described and discussed upon publication. Argon loss, alteration, resetting of the system at elevated temperatures and recoil (^{39}Ar loss) during neutron irradiation are common processes that may lead to underestimated or overestimated $^{40}Ar/^{39}Ar$ ages and must be appropriately evaluated in the produced datasets (e.g., McDougall & Harrison 1999). The existence of different standard calibration models (Kuiper et al. 2008; Renne et al. 2011) requires in depth knowledge of the method to be able to recalculate ages and directly compare $^{40}Ar/^{39}Ar$ data from different labs and/or older studies. Recalibration of previously published $^{40}Ar/^{39}Ar$ ages with different standards can lead to significantly younger or older ages (>0.5 Ma, see de Leeuw et al. 2018; Rocholl et al. 2017).

$^{40}Ar/^{39}Ar$ dating of volcanic ashes plays an important role in the establishment of a geological time frame for the sedimentary and volcanic successions. The Miocene history of the Central Paratethys was significantly affected by geodynamic processes in Central Europe; namely rollback of the subducted European slab, uplift of the Alpine–Carpathians–Dinarides fold and thrust belt and formation of extensional basins within the orogen. These processes were associated with intense volcanic activity, producing numerous Miocene intrusive and extrusive volcanic rocks (e.g., Pécskay et al. 2006; Harangi & Lenkey 2007; Lukács et al. 2018). Ashes of large volcanic eruptions are in some cases found more than 1000 km away from the source (e.g., Harsány ash; Lukács et al. 2018). So tuffs in the Central Paratethys record provide good opportunities for radio-isotopic dating, and in recent years the improved analytical precision resulted in high quality ages that enhance the chronostratigraphic framework of the Central Paratethys (de Leeuw et al. 2013, 2010; Rocholl et al. 2017; Bukowski et al. 2018).

The main aim of this paper is to point out the advantages of precise $^{40}Ar/^{39}Ar$ dating utilizing the high sensitivity mass spectrometer Argus VI+ by using three different tuff samples: The first tuff (PT4) from the Styrian Basin, previously dated with a previous generation mass spectrometer (VG-NG3600; Handler et al. 2006), was re-analysed to evaluate the potential age disparities. Another two samples of middle Miocene tuffs from the Vienna and Danube basin provided new age data that have a significant impact on the chronostratigraphic evolution of the western Central Paratethys (Badenian transgression, Badenian–Sarmatian Extinction Event). Special attention is paid to the difference between single and multiple grain measurements which were made possible by improvements of the analytical approach (i.e. a more sensitive mass spectrometer).

Methodology

Bulk ash samples were processed at the mineral separation facility of the Department of Earth Sciences of VU University Amsterdam in order to separate sanidine, biotite and hornblende grains for $^{40}Ar/^{39}Ar$ dating. Details on the separation processes for each sample are found in the supplementary data (Suppl. A). After checking the dried separates under an optical microscope, the sample from Pöls-1 (PT1) was not further processed, because the percentages of K-feldspar and biotite were extremely low. Moreover, the overall grain size was very small (< ~150 µm). From the Pöls-4 sample (PT4) transparent sanidine grains were handpicked under an optical microscope from the 90–200 µm fraction. The thickest, most angular hexagonal biotite grains without inclusions and visible alteration were handpicked from the PT4 (size 200–400 µm) and also from the Bernhardsthal-4 well samples (BE4; 200–250 µm and 250–500 µm fractions). Finally, clean hornblende grains were isolated from the Kamenica nad Hronom sample (KH2) and handpicked under an optical microscope (fraction 400–500 µm).

The selected mineral separates were packed in 6 mm ID Al (aluminum) packages and loaded together with Fish Canyon Tuff sanidine (FCs) standards in 25 mm ID Al (aluminum) cups. Samples and standards were irradiated at the Oregon State University TRIGA reactor in the cadmium shielded CLICIT facility for 18 hours (irradiation code VU109 [VU107 for biotite sample of PT4]). $^{40}Ar/^{39}Ar$ analyses were carried out on the ARGUS VI+ noble gas mass spectrometer at the geochronology laboratory of the VU University, Amsterdam. This is a high sensitivity, relatively low-resolution multi-collector noble gas mass spectrometer with an internal volume of 710 ml. The resolution of the system is ~200 and, therefore, it does not resolve hydrocarbon or chlorine interferences. The mass spectrometer is equipped with four Faraday cups at the H2, H1, AX and L1 positions and two compact discrete dynodes (CDDs) at positions L2 and L3. The system is equipped with a 10^{12} Ohm amplifier on H2 and 10^{13} Ohm amplifiers on H1, AX and L1 cups.

After irradiation, samples and standards were unpacked and loaded in a 185 hole Cu tray and baked overnight at 250 °C under vacuum. This tray was placed in a doubly pumped vacuum chamber with Zn-S window and subsequently baked overnight at 120 °C under high vacuum. The vacuum chamber is connected to a Thermo Fisher NGPrep gas purification line with four SAES-NP10 getters, a cold finger, an ion gauge, two inlets and two pipette systems. Samples were heated using a 25W Synrad CO_2 laser. The ARGUS VI+ has an NP10 getter and ion gauge on the source of the mass spectrometer. The NP10 getter is run cold and the ion gauge is turned off during analyses, because of its pumping capacity for argon. Sample gas was exposed to a Lauda cooler (−70 °C) and 2 cold and 1 hot (400 °C) NP10s for the September 2017 runs, and to a Lauda cooler (−70 °C), 2 cold NP10s and 1 hot (400 °C) NEG50 for the January 2018 runs. The samples were run on the H1-L3 collectors. Bias between the different detectors has been monitored by: 1) measurement of ^{40}Ar air pipettes across the different Faraday cups; 2) measurement of ^{40}Ar blanks on all detectors and 3) by measurement of mass 44 CO_2 in dynamic mode on all detectors. Bias between different cups was measured with air pipettes and/or CO_2 measurements (m/e 44) in dynamic mode yielding gain differences up to 14 % for different collectors. However, bias seems to be stable over weeks. Therefore, similar to Phillips & Matchan (2013), bias corrections were not applied and samples and standards were analysed in the same tray (and thus at more or less the same time) alternating with air pipettes of different intensities in the same range as the samples and standards. Line blanks were measured every 2–3 unknowns and were subtracted from the succeeding sample data.

In September 2017 single-grain fusion was performed on 25 sanidine grains of PT4 (90-200 µm), on 5 biotite grains of PT4 (200–400 µm), on 25 biotite grains of BE4 (200–250 µm) and on 24 biotite grains of BE4 (250–500 µm). An additional run in January 2018 included single and dual-grain fusions on 19 hornblende samples of KH2 (400–500 µm) and multiple-grain fusions (5–7 grains per hole) on 15 sanidine samples of PT4 and on 15 biotite samples of BE4 (250–500 µm). Data reduction was done in ArArCalc (Koppers 2002). Ages are calculated with Min et al. (2000) decay constants and 28.201±0.022 Ma for FCs (Kuiper et al. 2008). The atmospheric air value of 298.56 from Lee et al. (2006) is used. The correction factors for neutron interference reactions are $(2.64\pm0.02)\times10^{-4}$ for $(^{36}Ar/^{37}Ar)_{Ca}$, $(6.73\pm0.04)\times10^{-4}$ for $(^{39}Ar/^{37}Ar)_{Ca}$, $(1.21\pm0.003)\times10^{-2}$ for $(^{38}Ar/^{39}Ar)_K$ and $(8.6\pm0.7)\times10^{-4}$ for $(^{40}Ar/^{39}Ar)_K$. All errors are quoted at the 2σ level and include all analytical errors. All relevant analytical data for age calculations can be found in the online supplementary material B.

In general, the ^{40}Ar (and ^{38}Ar and ^{36}Ar) blank measurements of the samples measured in January 2018 have lower values and a lower amount of scatter than the ones from September 2017. The occasional instability of the blank measurements in September was caused by a very tiny leak in the electrical feed troughs of the NP10 getter when it was run at 400 °C ("air burps" up to 10fA in periods of hours-days). Replacing this NP10 getter with a NEG50 getter for the 2018 measurements resulted in more stable blank values. The lower ^{40}Ar blank values in 2018 than in 2017 are the result of the progressive cleaning of the partly new system with time.

From the analytical point of view, the weighted mean age calculations include the most reliable sample data. First of all, they must contain a relatively high percentage of radiogenic ^{40}Ar (preferably $^{40}Ar^* > 75$ %) to minimize impact/influence of potential alteration of minerals. Note that the $^{40}Ar^*$ content for several samples is >100 %, which is the result of very low ^{36}Ar intensities around the detection limit of the extraction system and the mass spectrometer. This sometimes results in negative values of ^{36}Ar (i.e. preceding blank was slightly higher in intensity than sample). One could argue for forcing all negative intensities to zero. However, analytical uncertainties related to ^{36}Ar measurement are then ignored in error propagation leading to very small analytical uncertainties. It was preferred to include these negative intensities and incorporate analytical uncertainties related to our ^{36}Ar measurement.

The mineral composition of PT4 sample was analysed under polarizing microscope and under the Cameca SX 100 microprobe (State Geological Institute of Dionýz Štúr, Bratislava, Slovakia). The sample is strongly expandable due to alteration to swelling clay minerals, which limited preparation of thin sections. Minerals were measured using WDS analysis with accelerating voltage 15 keV, probe current 20 nA with a beam width of 10 μm. Raw analyses were recalculated to weight percent of oxide using the ZAF correction. Other minerals were determined by EDAX analyses.

Geological background of the sampled horizons

The semi-isolated Paratethys Sea covered large areas of Central and Eastern Europe during the early-middle Miocene (e.g., Rögl 1998; Popov et al. 2004). It occupied a chain of sub-basins with environments controlled by tectonics, climate and sea-level change (e.g., Harzhauser & Piller 2007; Popov et al. 2010). The western part of the Central Paratethys included the Alpine–Carpathian Foredeep, Vienna Basin and partially the Pannonian Basin System (Fig. 1). These depocenters have been essentially formed by east–west extension driven by slab rollback since ~18 Ma (Tari et al. 1999; Horváth et al. 2006; Mandic et al. 2012; Lukács et al. 2018). The basins were also affected by shear and compression, caused by the uplift and escape of tectonic terranes of the Eastern Alps and Western Carpathians (e.g., Kováč et al. 2017). During the middle Miocene, several key events are known to have significantly influenced the depositional and biostratigraphical record; notably the Badenian transgression, the Badenian salinity crisis and the Badenian–Sarmatian Extinction Event (Piller et al. 2007; de Leeuw et al. 2010, 2018; Sant et al. 2017).

The Badenian is the regional stage of Central Paratethys, corresponding in age to the Langhian and early Serravallian of the standard Geological Time Scale (e.g., Hilgen et al. 2012). The ages for the key paleoenvironmental changes that took place in the Badenian have recently been revised and are seriously debated (e.g., Kováč et al. 2007, 2017; Hohenegger et al. 2009, 2014; Sant et al. 2017, 2019). The new $^{40}Ar/^{39}Ar$ ages come from three volcanic horizons that are intercalated in middle Miocene successions (Fig. 1): 1) Tuff from Kamenica nad Hronom; (Pozba–Vráble formations, Danube Basin), 2) tuffite from the Bernhardsthal-4 well (base of Jakubov Formation, Vienna Basin), 3) Tuff from the Quellgraben section in Pöls (Florian Formation, Styrian Basin).

Tuff from the Quellgraben section in Pöls (Florian Formation, Styrian Basin)

The Quellgraben section in Pöls is located in the western Styrian Basin (Austria), ca. 250 m E of the village of Pöls an der Wieserbahn (46°53'38.3"N, 15°24'38.6"E). The outcrop was first described in detail by Kopetzky (1957). Two tuff layers are present in the lower part of the section (Fig. 2). The section starts with mica- and gastropod-rich sandy marls which are overlain by the first tuff layer (PT4). Silty, muscovite-rich fine sands and sandstones follow. Section continues with 85 cm thick layer of reddish tuffitic marls. The second ash layer (PT1 – not used for dating) occurs in the lowermost part of these tuffitic marls. In the upper part of the section, the marls gradually pass into well-sorted sands and sandstones commonly containing articulated bivalves. The section only yields benthic foraminifera, while the planktonic foraminifera were not observed. Diatoms are very abundant. The calcareous nannoplankton assemblage is composed only from non-markers and reworked species (*Reticulofenestra haqii, Prediscosphaera cretacea* and *Rucinolithus* sp.).

The marly sediments of the Quellgraben section belong to the Florian Formation (Nebert 1989; Piller et al. 2004). This unit is correlated to the lower Badenian Lagenidae Zone (Langhian; Kopetzky 1957; Kollmann 1965; Ebner & Gräf 1977; Balogh et al. 1994; Handler et al. 2006). Handler et al. (2006) presented $^{40}Ar/^{39}Ar$ dating on the PT4 sample with an age of 15.75±0.17 Ma (as originally reported, not recalibrated). Radio-isotopic dating of the tuff agrees with cor-

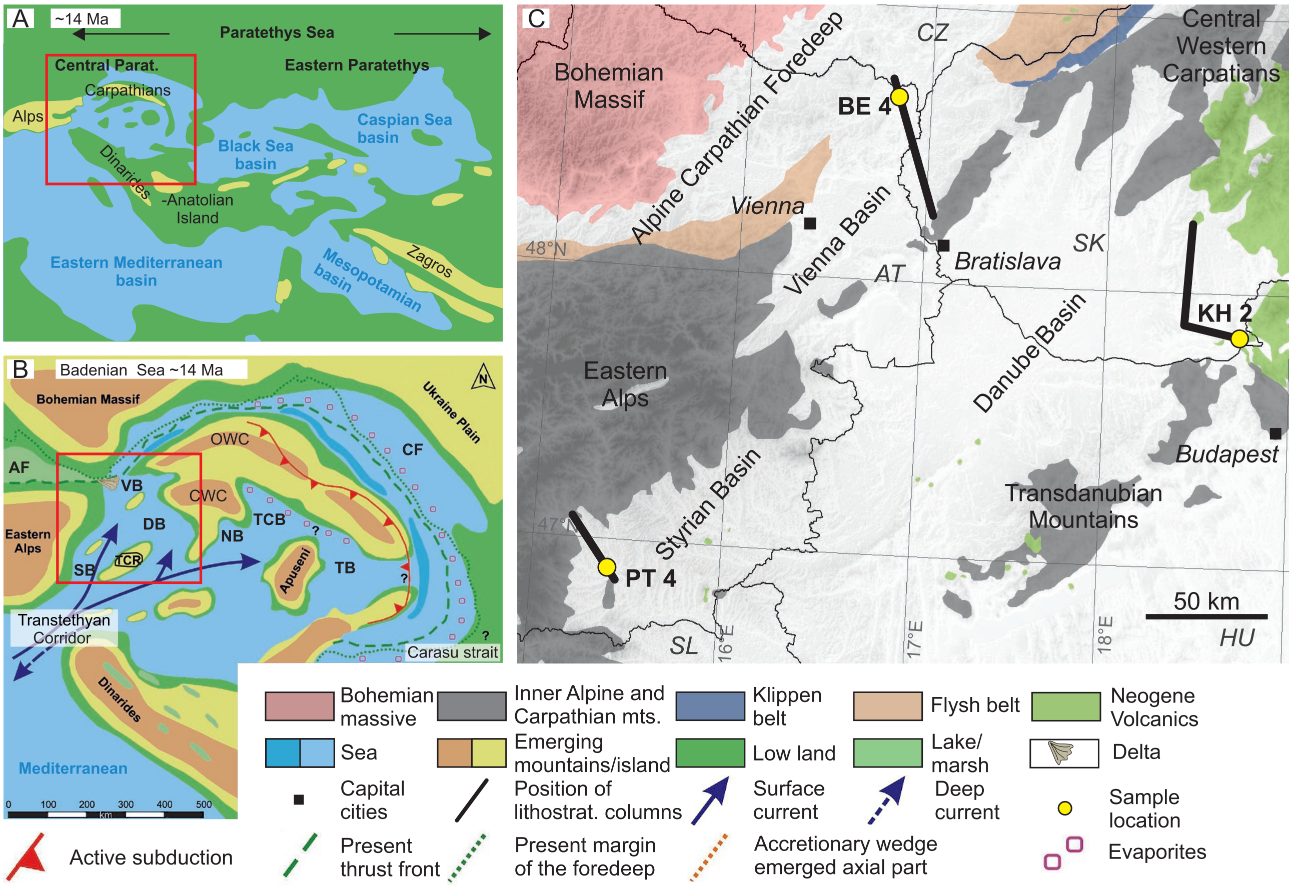

Fig. 1. A — Overview of the Paratethys and Mediterranean basins during the Middle Miocene. **B** — Configuration of sediments and sea during the Badenian in the Central Paratethys Sea after Kováč et al. (2017). **C** — Location of the studied sections, with marked position of lithostratigraphic columns; PT4=Quellgraben in Pöls, BE4=Berhardsthal 4 well, KH2=Kamenica nad Hronom; DB — Danube Basin, VB — Vienna Basin, SB — Styrian Basin, TCB — Transcarpathian Basin, TB — Transylvanian Basin, CF — Carpathian Foredeep, AF — Alpine Foredeep, OWC — Outer Western Carpathians, CWC — Central Western Carpathians, TCR — Transdanubian Range.

relation to the Florian Formation. The re-sampled tuff (PT4) is bentonitized, and composed of K-feldspar, biotite, quartz, zircon, strongly altered grains in mass of bentonite clays. K-feldspars are formed by fresh sanidine (Or_{67-69}) without mineral inclusions (Fig. 3a; Appendix). However, one orthoclase grain was also recognized ($Or_{95.5}$). Altered grains probably belong to K-feldspar (Sanidine) altered into a mixture of secondary quartz and phyllosilicates (Fig. 3b). Biotite crystalloclasts are chloritized. Plagioclase was not found, and it is likely that it has been transformed into clay.

Tuffite from the Bernhardsthal-4 well (Jakubov Formation, Vienna Basin)

The first well-bound tuffite layer from the Vienna Basin that was cored and became available for analysis is reported from the Bernhardsthal-4 well (48°41'15.62"N, 16°51'12.66"E). It is situated within the Bernhardsthal oil field in the Austrian part of Vienna Basin, close to the Czech boundary (Figs. 1, 4). The discontinuous cores were made accessible by OMV for sampling. A piece of core (~80 cm^3) with the tuffite layer (BE4) was used for $^{40}Ar/^{39}Ar$ dating. A petrographic study was not applied here, because the whole sample was required for the age dating procedure.

The Bernhardsthal-4 well includes 2480 m of Neogene deposits, which rest discordantly on the Rhenodanubian Flysch (Harzhauser et al. 2018). The studied layer (depth of 2295–2300 m) forms the base of an ~100 m thick unit of grey, clayey fine sandstone, intercalated between deep water deposits of the Lužice Fm. (middle Burdigalian/Ottnangian Stage) and shallow water deposits of the Jakubov Fm. (lower Badenian/Langhian). Within this interval the microfauna is unfortunately represented by strongly recrystallized, unidentifiable planktonic foraminifera.

Tuff from the Kamenica nad Hronom section (Pozba–Vráble formations, Danube Basin)

The outcrop is located in an abandoned quarry at the westernmost end of the Kamenica nad Hronom village close to the Hron River mouth (47°49'50.38"N, 18°42'39.26"E). The section is 31 m thick and its basal part is composed of

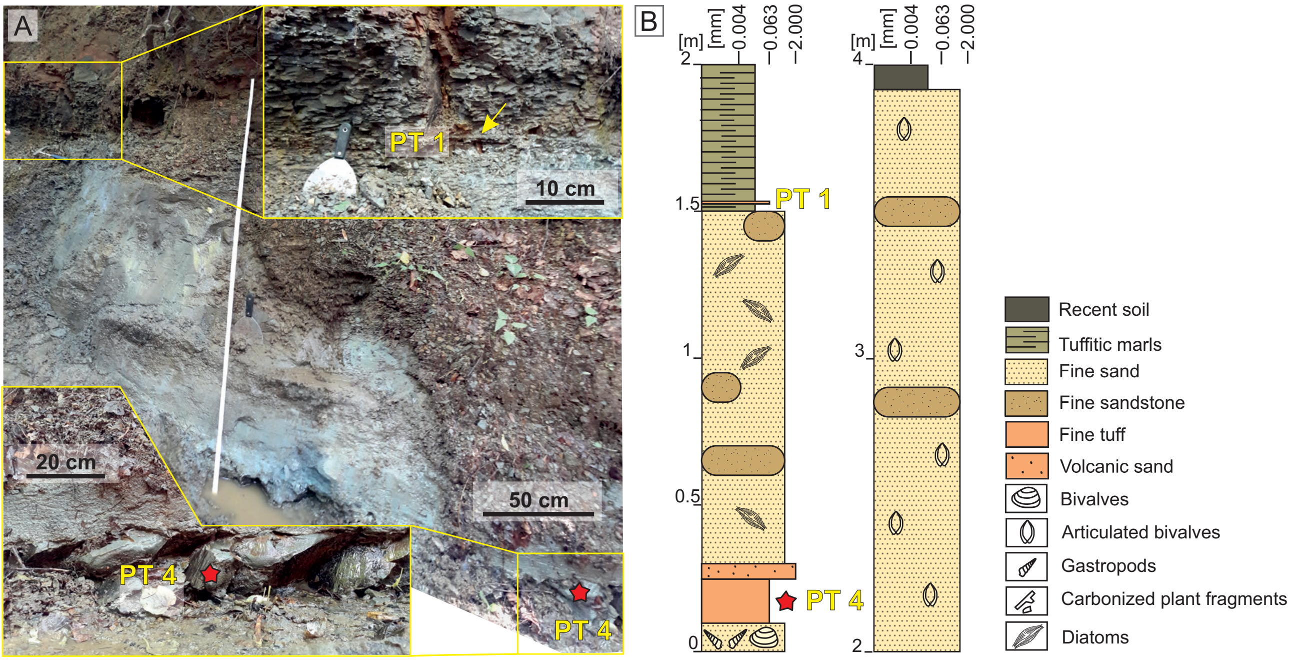

Fig. 2. Quellgraben in Pöls: **A** — Outcrop photo; **B** — Lithological logs. Sample positions (PT4) indicated by an asterisk.

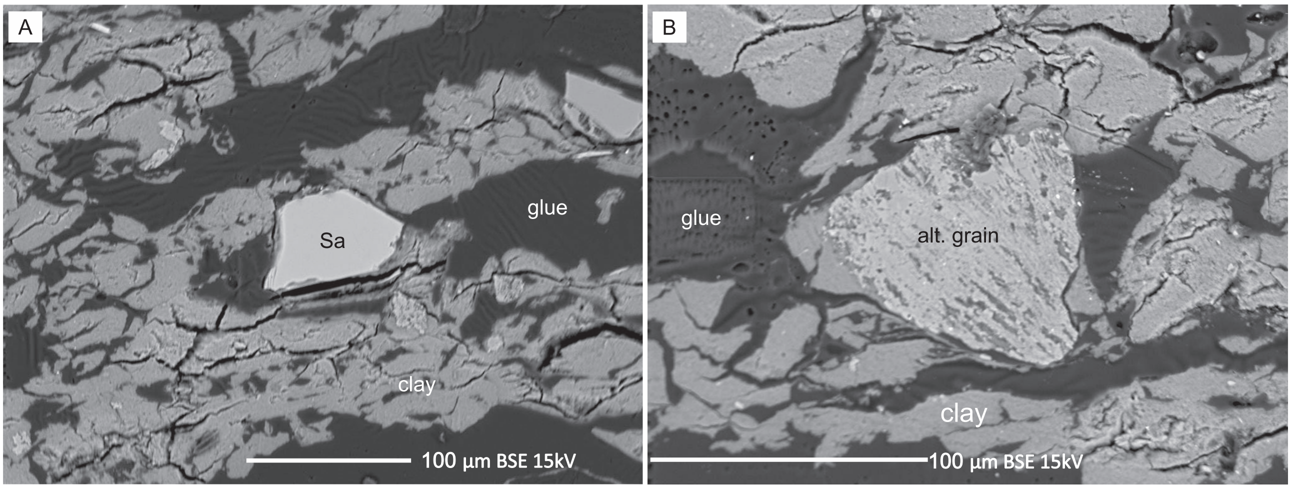

Fig. 3. BSE image of PT4 sample: **A** — Sanidine (analyse-1); **B** — Altered grain; light grey colour represents the clay groundmass and dark grey colour represents glue.

volcanic conglomerate (Fig. 5a,c). The conglomerate is covered by lapilli tuffs to tuff breccia, where subaquatic environment is indicated by abundant porifera spicules (Nováková et al. in press). The tuff breccia is overlain by well rounded, poorly sorted conglomerates, followed by the sampled tuff layer with fossil leaves on the top. The sampled tuff layer passes into lapilli tuff, which is covered by boulder-size conglomerates with remnants of loess at the top of the section (Nováková et al. in press). Additionally, in the neighbouring Shooting gallery outcrop (47°50'32.29"N, 18°43'55.62"E), the andesitic conglomerate is covered by fossiliferous sandstones, which also formed lenses within the conglomerate (Fig. 5b,d). Fossiliferous sandstones contain taxa associated with the calcareous nannoplankton NN6 Zone (Vaškovský et al. 1982; Nováková et al. in press).

This area belongs to the Visegrád–Börzsöny–Burda volcanic field (Balogh et al. 1981, 1998; Karátson et al. 2000; Pécskay et al. 2006; Bezák et al. 2009; Lexa et al. 2010). The volcano-sedimentary complex of andesitic conglomerate in the lower part of outcrop is traditionally correlated with the lower Badenian Burda Fm. and represents volcanic activity in shallow marine conditions (Seneš et al. 1962; Vaškovský et al. 1982; Vass 2002; Bezák et al. 2009; Lexa et al. 2010). The Burda Fm. laterally passes into mudstones and sandstones of the Bajtava–Špačince Formation, which contains calcareous nannofossil species of the NN5 biozone, together with

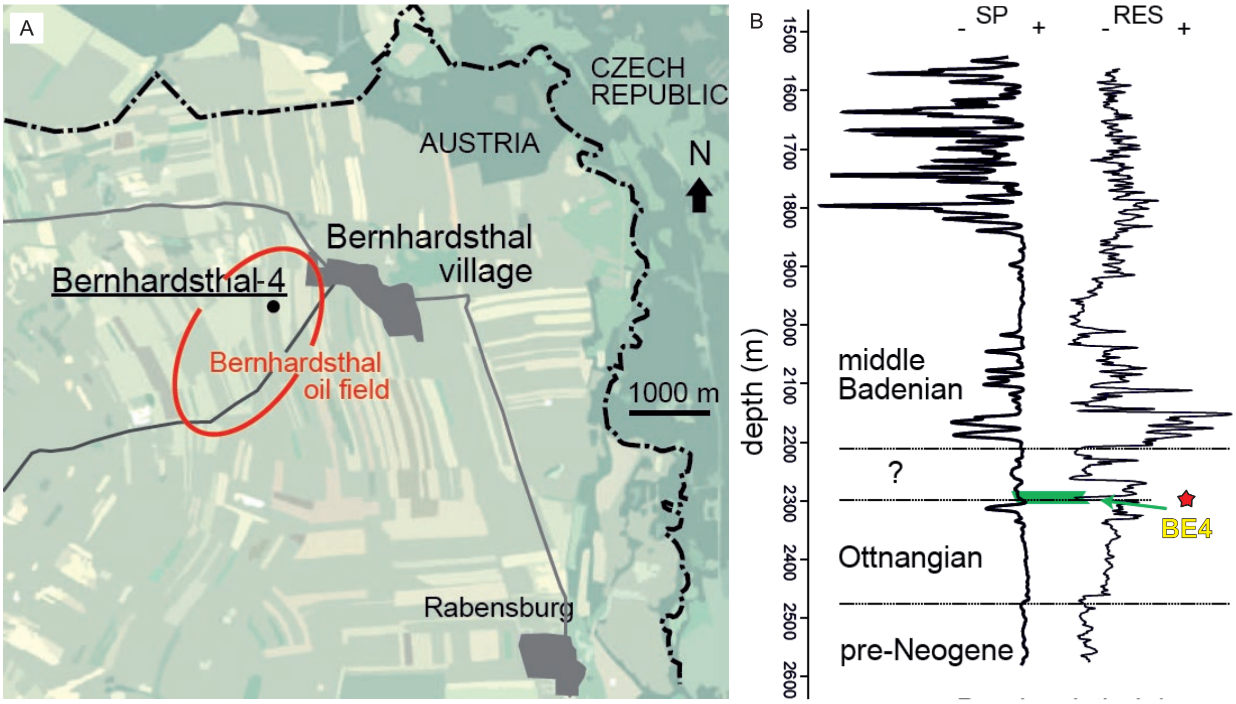

Fig. 4. Bernhardstahl-4 well: **A** — Map position. Sample positions (BE4) indicated by a black dot. **B** — Well logs (well log data have been log-transformed and smoothed with a Gaussian filter). Sample position (BE4) indicated by an asterisk.

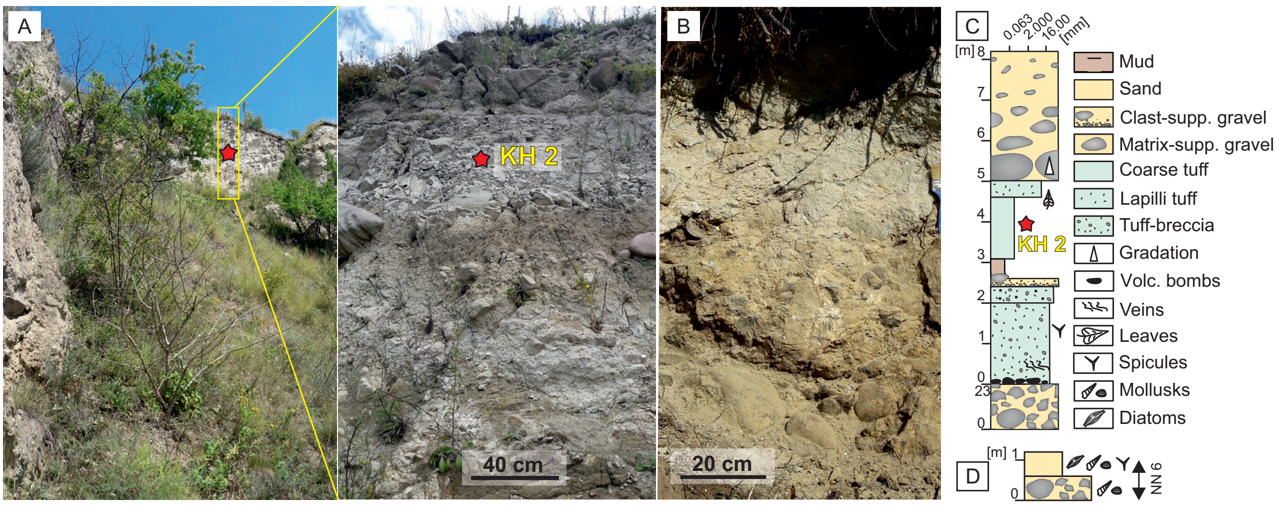

Fig. 5. Kamenica nad Hronom: **A** — Dated section with position of KH2 indicated by an asterisk; **B** — Shooting gallery section; **C+D** — Lithological log of both sections.

the planktonic foraminifera *Orbulina suturalis* (Vass 2002; Kováč et al. 2018). Based on the presence of the NN6 Zone, sediments above andesite conglomerate can be attributed to the late Badenian–Sarmatian (Serravallian) Pozba–Vráble formations.

The tuffs selected for dating (KH2; Fig. 5a) represent deposits of a pumice-ash pyroclastic flow (Bezák et al. 2009). The andesite tuffs consist of pumice fragments, crystalloclasts of plagioclase (An_{88-83} core; An_{52-66} rim), biotite, brown-green amphibole and of volcanic lithoclasts in tuffaceous matrix (Nováková et al. in press). The volcanic lithoclasts with porphyric texture are composed of microlithic groundmass with plagioclase, biotite and amphibole phenocrysts. Pseudomorphs of pyroxene shape are rare. On the basis of their chemical composition, amphibole can be divided to two groups: hastingsite–sadanagaite and hornblende. Hornblende can be considered as juvenile. Hastingsite to sadanagaite was probably sourced from underlying lapilli tuffs and older volcanic rocks. Nonvolcanic admixture is represented by polycrystalline quartz, paragneiss, granitoid and siltstone clasts. For radio-isotopic analyses, 5 dm^3 bulk samples were taken.

Results

$^{40}Ar/^{39}Ar$ analysis and ages of the Pöls tuff (PT4)

The two different sets of sanidine age data from PT4 (single grain: K12a; multiple grain: K12b) show a similar scatter in ages with the largest group between ~14 and 15.3 Ma, and some grains between ~16 and 17 Ma (Fig. 6a). The main difference between the $^{40}Ar/^{39}Ar$ results of the single versus multiple grain is the beam intensity ^{40}Ar. Unsurprisingly, this is higher in the multiple grain measurements, because the sample volume is larger. It is clear that the ^{40}Ar amount in the single grains was around the detection limit of the ARGUS mass spectrometer and its extraction line at time of measurement: the total measured ^{40}Ar is regularly in the same order as the blank measurement, resulting in a lower precision than for the multiple grain measurements. The single grain data, however, agree very well with the multiple grain data, apart from having a larger uncertainty.

Age calculations only include samples with a $^{40}Ar^*$ percentage >75 % and ^{37}Ar signals below 1 fA. High ^{37}Ar values reflect high Ca-content pointing to plagioclase instead of K-feldspar. Although plagioclase can be dated reliably, due to its low K content, incorporation of excess argon possibly effects measured data yielding anonymously old ages (McDougall & Harrison 1999 and references therein). In addition, neutron interference corrections are more substantial for plagioclase (due to the $^{40}Ca(n,n\alpha)^{36}Ar$ and $^{42}Ca(n,\alpha)^{39}Ar$ reactions during irradiation) yielding larger analytical uncertainties (McDougall & Harrison 1999). Argon retention in plagioclase is also sometimes problematic (McDougall & Harrison 1999). The weighted mean age (assumed to be the age of the volcanic eruption) is based on the youngest grains that define a plateau and data are included as long as the mean weighted standard deviation (MWSD) is <statistical T-test at a 95 % confidence level. Given these strict requirements, the weighted mean age for the single grain dataset (K12a) is **14.31±0.27 Ma** (n=4). One cluster of analytically reliable older data exists in the age range of 15.04±0.36 and 15.32±0.29 Ma (Fig. 6).

For the multi grain measurements (K12b), the total measured ^{40}Ar is 4 to 22 times larger than the procedure blank and, consequently, analytical uncertainties are much lower, showing that the analytical quality of this dataset is potentially much higher. At the same time, the drawback of the multiple grain dataset is that the calculated ages per sample reflect the average of 5–7 sanidine grains, so it is not possible to see the full geological scatter of ages within the sample. The mean age based on the multiple grain dataset (K12b) is **14.03±0.04 Ma** (n=4), which overlaps statistically with the average for the single grain dataset. The full age range including the most reliable samples (n=8) is: 13.98±0.06 Ma to 14.26±0.11 Ma *(13.92 to 14.37 Ma)*. In addition, the dataset contains three older grains in the age range of ~16–17 Ma, but their very low $^{40}Ar^*$ percentages (29–36 %) might indicate alteration. For all mean ages, the $^{40}Ar/^{36}Ar$ ratios (isochron intercepts) overlap with the expected atmospheric composition (Lee et al. 2006; Fig. 6 b,c).

In summary, the most conservative interpretation of the $^{40}Ar/^{39}Ar$ data of the PT4 tuff, based on the full range of all reliable single and multiple sanidine measurements, gives an age range between 13.98±0.06 Ma and 14.47±0.56 Ma (~13.9–15.0 Ma), but the geological age is most probably at the lower end of this range below 14.5 Ma (< 14.31±0.27 Ma).

The small set (n=5) of single grain biotite measured from the PT4 sample (K2) has relatively low ^{40}Ar beam intensities (2.5–28.7 fA) and, more importantly, also low $^{40}Ar^*$ percentages (11–70 %). Low $^{40}Ar^*$may point to alteration (i.e. possible argon loss, and thus younger ages). This is also supported by the microprobe analysis. The ages of the four oldest grains agree with the majority of the sanidine ages (~14 to 15.2 Ma; Fig. 6).

$^{40}Ar/^{39}Ar$ analysis and ages of the Bernhardsthal-4 tuff (BE4)

The single grain data (K14: 200–250 μm, and K13a: 250–500 μm) from biotites of BE4 have much larger error bars than the multiple grain measurements (K13b: 250–500 μm). This is a direct result of their lower sample volume resulting in a lower amount of ^{40}Ar, only 1 to 5 times larger than the ^{40}Ar measured in the blanks (Fig. 7).

The age ranges from the large and small grain fractions are comparable (~14.1 to 17.1 Ma), but grains from the smaller grain size fraction are in most cases slightly older. Differences in ages for different grain sizes may be caused by differential crystallization processes in the magma chamber, although the temperatures of magma systems are generally higher than closure temperatures for argon diffusion out of a mineral. Usually the larger grains start recrystallizing earliest, and should, therefore, be slightly older than the smaller grains (Andersen et al. 2017). This, in combination with biotite closure temperatures around ~300 °C (Hora et al. 2010), is opposite to our observations, so this most likely did not play an important role for the biotite BE4 sample. A more likely cause to explain the observed difference is the loss of ^{39}Ar during recoil (e.g., Turner & Cadogan 1974; Onstott et al. 1995). This effect is usually most dominant in grains with relatively large surfaces compared to their total volume, namely thinner and smaller grains (sheet silicates). The larger grain size fraction (K13) contained generally thicker grains than the smaller fraction (K14), which might explain the generally older ages for the latter. Hence, the data from the smallest grain size fraction are considered to be less representative for the geological age of the BE4 sample.

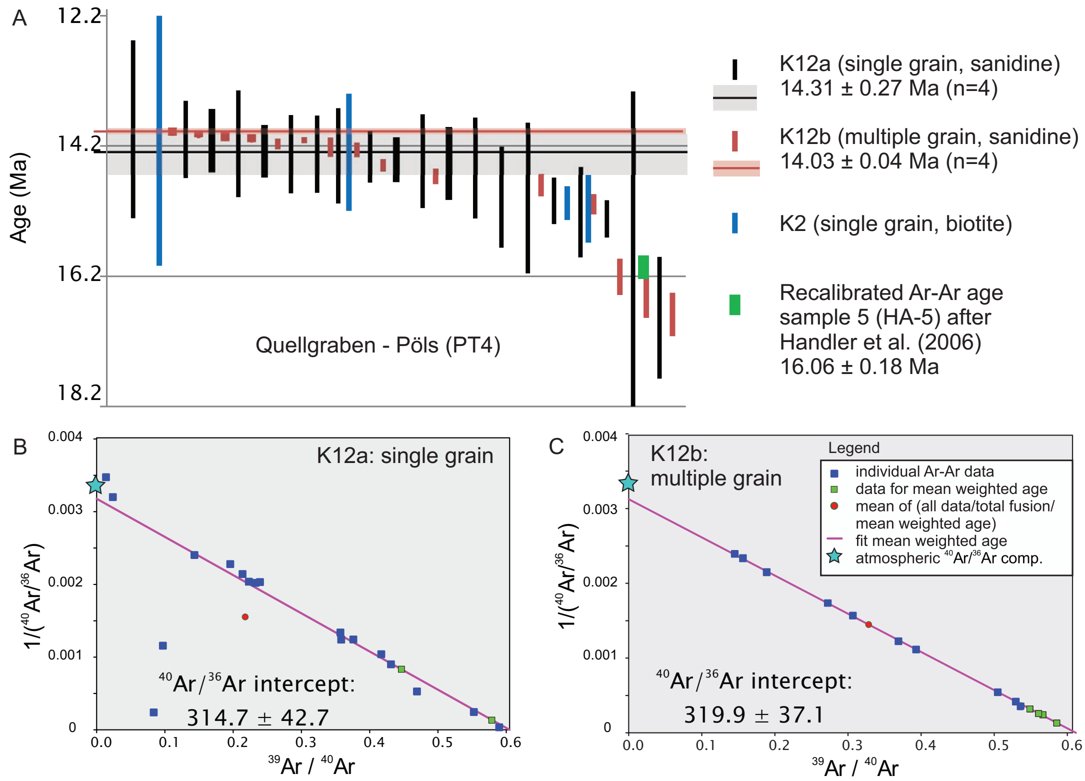

Fig. 6. A — Summary of $^{40}Ar/^{39}Ar$ ages with error bars for different groups of grains of sample PT4 including the recalibrated age of Handler et al. (2006). See also Table 1. Samples included for the weighted mean age are indicated by a thicker line. **B, C** — Inverse isochrons of the multiple grain and single grain sanidine data sets. The pink line is defined by the grains included for the mean weighted age calculation. The asterisk represents the atmospheric $^{40}Ar/^{36}Ar$ composition. All errors are cited at 2σ.

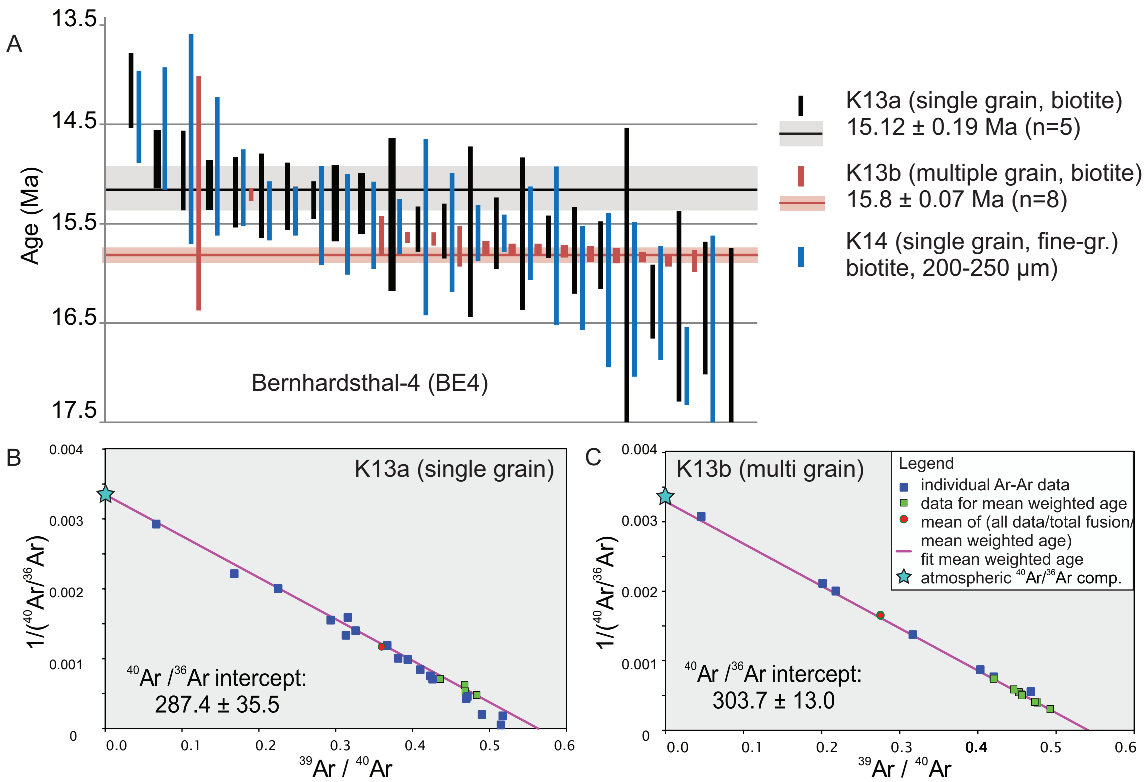

Fig. 7. A — Summary of $^{40}Ar/^{39}Ar$ ages with error bars for different groups of grains of sample BE4. Samples included for the weighted mean age are indicated by a thicker line. **B, C** — Inverse isochrons of the multiple grain and single grain biotite data sets of fractions 250-500 μm.

It is striking that the single grain dataset (K13a) has a much wider age range (~14.1 to 17 Ma) than the multiple grain set (~15.2–16 Ma; Fig. 7). The weighted mean age of the single grain data set (**15.12±0.19** Ma; n=5; >75 % ^{40}Ar), defined by the youngest group of ages with MWSD<statistical T-test, is much younger than that of the multiple grain dataset. The multiple grain set (K13b) has one reliable age at 15.20±0.07 Ma, followed by an older group of ages with a weighted mean age of **15.8±0.07 Ma** (n=8, >75 % ^{40}Ar*). The ^{40}Ar/^{36}Ar ratios for all weighted mean ages overlap with the expected atmospheric value (Lee et al. 2006), suggesting that potential ^{40}Ar gain is of minor importance for the biotites in this dataset (e.g., Hora et al. 2010; Fig. 4b,c).

The data from the multiple grain measurements are clearly more robust from an analytical perspective, but one should take into account that the age result per sample represents an average of 5–7 biotite grains. When a tuffite sample has grains with a wide range of geological ages, multiple grain measurements will most frequently represent age values around the median of this age range that is not necessarily its eruption age. This also seems to be the case for the BE4 sample. The relatively low age of 15.2 Ma for one reliable multiple grain sample confirms that several younger grains are present in the fraction (Fig. 7). Hence, the reliable single grain measurements (^{40}Ar*>75 %) on the large grains (K13a) give us the best insight into the full age range of the BE4 tuffite. This age range being 14.85±0.29 Ma to 16.33±0.96 Ma.

^{40}Ar/^{39}Ar analysis and age of Kamenica nad Hronom tuff (KH2)

The ^{40}Ar/^{39}Ar results of the hornblende grains of KH2 sample are characterized by low percentages of radiogenic ^{40}Ar (<62 %) and very low K/Ca values (Fig. 8). This is in line with the composition of the hornblende which naturally has a low K concentration, resulting in lower amounts of daughter isotope ^{40}Ar. Low amounts of ^{40}Ar* might suggest alteration with possible loss of argon from the minerals. Relatively large Ca-corrections for neutron interference reactions are needed (through measurement of ^{37}Ar) as a result of larger analytical errors on the dataset.

The precision of the KH2 measurements is good and the spread in ages of the tuff, in this case based on samples with ^{40}Ar* >20 %, is relatively small: ~12.4–13.2 Ma. Some of the single grain measurements have relatively large uncertainties, but show the same trend as the data based on the fusion of two grains. The weighted mean age, based on the youngest group of ages using the MSWD<statistical T-test criterion, is **12.56±0.10 Ma** (n=10). The ^{40}Ar/^{36}Ar normal isochron intercept value of 298.7±2.6 is very close to the expected atmospheric ratio after Lee et al. (2006; 298.56), suggesting that no excess Ar was incorporated (Fig. 8b). This suggests that despite the very low K and Ar amounts and high Ca amounts, the mean age of KH2 is close to the eruption age of the tuff.

The results of the hornblende sample (KH2) from Kamenica nad Hronom in the Danube Basin are in line with other ^{40}Ar/^{39}Ar studies on amphiboles. Despite low ^{40}Ar* percentages and relatively high ^{37}Ar values, hornblende samples generally yielded good results with a high release of ^{39}Ar, stable Ca/K ratios and ^{40}Ar/^{36}Ar intercept values overlapping with the atmospheric value (e.g., Dilek et al. 1999; Çelik et al. 2011; Parlak et al. 2013; Daşçi et al. 2015). Note that the relatively long irradiation time of 18 hours helped to generate a sufficient ^{39}Ar for analysis.

Improvements in geochronology: single versus multiple grain ^{40}Ar/^{39}Ar ages

The weighted mean ages of PT4 based on both the single and multiple grain ^{40}Ar/^{39}Ar measurements presented in this study (14.31±0.27 Ma and 14.03±0.04 Ma, respectively) are much younger than the previously published ^{40}Ar/^{39}Ar plateau age of 15.75±0.17 Ma from the Pöls section (Handler et al. 2006). The latter age is based on one stepwise Ar/Ar fusion measurement containing two large feldspar grains (0.5–1.0 mm size). The Ar-release patterns of the plateaus comprising 91.9 % of the released $^{39}Ar_K$ suggest a reliable measurement. The used standard (DRA1 sanidine of 25.03 Ma) and the decay constants (Steiger & Jäger 1977) differ from the values in the calibration models that are currently often applied and also from the ones used for the presented study. Therefore, the data were recalibrated according to the calibration model of Kuiper et al. (2008) using the Min et al. (2000) decay constants and Fish Canyon tuff sanidine in order to compare them directly to the new ^{40}Ar/^{39}Ar data from this study (Table 1). The Drachenfels age is originally based on the 24.99±0.07 Ma reported in Wijbrans et al. (1995) relative to 27.92 Ma Taylor Creek Rhyolite sanidine (TCs) and using Steiger & Jäger (1977) decay constants. In combination with the inter-calibration factor 1.0112±0.0010 for the Fish Canyon Tuff sanidine (FCs) and TCs from Renne et al. (1998), and with the FCs of 28.201±0.022 Ma of Kuiper et al. (2008) relative to Min et al (2000), this converts to 25.52±0.08 Ma that is used here to recalibrate the ages by Handler et al. (2006).

The recalibrated age for the Quellgraben tuff is **16.06 ±0.18 Ma**, which is older than the previous age. For simplicity, it will be henceforth referred to as HA-5 from Handler et al. (2006; Sample 5). Remarkably, the study by Handler et al. (2006) describes the minerals in HA-5 as sanidine (K-feldspar), while the relatively high ^{37}Ar/^{39}Ar ratio compared to their other measurements on biotite (~2 versus ~0.1) show that the feldspars yielded high ^{37}Ar signals, which is characteristic for a Ca-rich and K-poor fraction (e.g., plagioclase, Ca-feldspar). This is also supported by the relatively low ^{40}Ar* (%) yields. In general, Ca-feldspars give less reliable dating results than sanidine, which might result in overestimated ages. Nevertheless, the published ^{40}Ar/^{36}Ar rate (isochron intercept) for HA-5 is close to the expected atmospheric air value (Lee et al. 2006) suggesting a low extraneous ^{40}Ar yield.

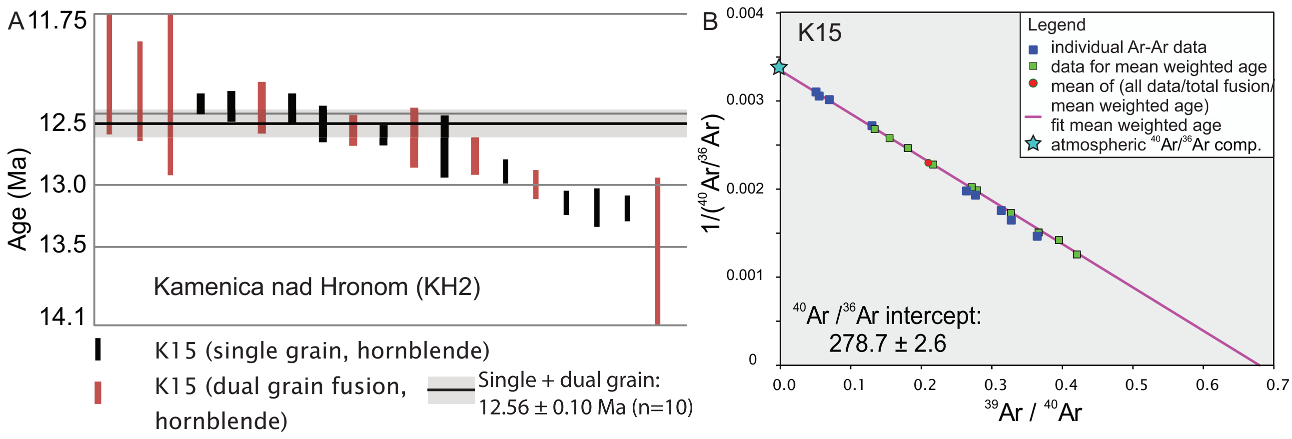

Fig. 8. A — Summary of $^{40}Ar/^{39}Ar$ ages with error bars for different groups of grains of sample KH2; **B** — Inverse isochron.

Table 1: Recalibrated $^{40}Ar/^{39}Ar$ ages of Handler et al. (2006). Note: Error calculation could not be applied in full detail, since the sources of uncertainty in Handler et al. (2006) were not completely described. For the recalibration, the percentage error in the age was transferred to R and used to calculate the new age ($R=[^{40}Ar^*/^{39}Ar_K]$ sample/$[^{40}Ar^*/^{39}Ar_K]$ standard; see Renne et al. 1998).

	old age (Ma)	old error (Ma)	R	error	new age (Ma)	new error (Ma)
Sample 1 (Retznei)	14.21	0.07	5.66E−01	2.79E−03	14.49	0.08
Sample 2 (Retznei)	14.39	0.12	5.73E−01	4.78E−03	14.67	0.13
Sample 3 (Hörmsdorf)	15.08	0.09	6.01E−01	3.59E−03	15.38	0.10
Sample 4 (Hörmsdorf)	15.22	0.17	6.06E−01	6.77E−03	15.52	0.18
Sample 5 (Pöls/HA-5)	15.75	0.17	6.28E−01	6.77E−03	16.06	0.18

The age of the HA-5 sample was based on a single measurement of two feldspar grains, so the contribution to the mean age per grain cannot be distilled. The $^{40}Ar/^{39}Ar$ plateau age of HA-5 corresponds to the oldest set of grains from sample PT4, both visible in the single and multiple grain fusions (Fig. 6). The grains in this set yield low radiogenic $^{40}Ar^*$ percentages (<35 %) and some were relatively rich in calcium. It is possible that one or both feldspars from sample HA-5 belonged to the same group of potentially altered grains or grains with adhering clays. In any case, the age of HA-5 most likely does not represent the geological age of the Florian Formation sediments.

The advantage of the presented $^{40}Ar/^{39}Ar$ dataset (sample PT4) in this study compared to the pilot study by Handler et al. (2006) is that the larger number of measurements gives insight into the distribution of ages within the tuff sample. The full dataset (single and multiple grain) is clearly a mixture of more or less pristine and (slightly) altered sanidine grains together with some Ca-clay impurities, as suggested by the large variation in measured isotope intensities (i.e. fluctuating $^{40}Ar^*\%$ and ^{37}Ar) and ages. It also suggests that some reworking has taken place, because even the analytically most reliable samples show a relatively wide age range (~14.1 to 15.3 Ma; Fig. 6). We can conclude that the most reliable age of the PT4 tuff is between 15.0 and 13.9 Ma, and more specifically between 14.31±0.27 Ma and 14.03±0.04 Ma.

Implications for the middle Miocene evolution of the Central Paratethys

The Badenian flooding of the Styrian Basin

Current bio- and magnetostratigraphic studies imply that the initial Badenian flooding of the Styrian Basin was marked by a short transgressive event on top of an angular unconformity of Karpatian age, dated to ~16.3 Ma, after which regression and erosion of the marginal facies took place (Ebner & Sachsenhofer 1995; Schreilechner & Sachsenhofer 2007; Hohenegger et al. 2009, 2014; Spezzaferri et al. 2009). This was followed by a second transgression ~14.8 Ma, which established a long lasting marine environment in the marginal parts of the Styrian basin (Rögl et al. 2002; Hohenegger et al. 2009). The preceding age of HA-5 (15.75±0.17 Ma) for the Florian Fm. was used by Hohenegger et al. (2009) as a supplementary tie point (besides biostratigraphy) for their magnetostratigraphic correlation of the basal marine Badenian interval in the Wagna section (based on regional stratigraphic correlation) to Chron C5Br (15.974–15.16 Ma). The younger age range for the same tuff (14.31±0.27 Ma and 14.03±0.04 Ma) obtained here, however, suggests a different scenario. It indicates that the Pöls tuff is roughly synchronous with the Retznei quarry tuff (Reuter et al. 2012; recalibrated Ar–Ar age from Handler et al. 2006: 14.49 Ma and 14.67 Ma, Table 1) and that the transgressive base of the Wagna section should be correlated to a younger interval of the time scale such as C5Bn.2n and C5Bn.1r (15.16–14.87 Ma). The latter correlation agrees with a recent data compilation of the onset of the Badenian Sea presented by Sant et al. (2017), showing that the base of the Badenian flooding (associated with planktonic foraminifer *Praeorbulina*) is younger than 15.3 Ma when the modern Mediterranean taxonomy and biochronology are applied. The first occurrence of *Praeorbulina,* present in the basal Badenian sediments of the Wagna section (Hohenegger et al. 2009), has an age of 15.2 Ma according to Mediterranean biochronology (see Sant et al. 2017). This, together with the younger age data of the Quellgraben tuff in Pöls, supports an overall younger age of the onset of the Badenian Sea in the Styrian Basin (<15.3 Ma), which significantly differs from the late early Miocene age (~16.3 Ma) established by previous studies (Hohenegger et al. 2009, 2014).

The revised age for the Florian Fm. is in agreement with the regional lower Badenian stage sense Papp et al. (1978) and the Lagenidae Zone of the Central Paratethys, which has a maximum age range of 16.3 to 13.8 Ma (Hohenegger et al. 2014). It implies that the shallow marine Florian Fm. is slightly older or time equivalent with the carbonate platforms of the Weissenegg Fm. exposed in the Retznei quarry, and time equivalent or younger than the top of the Wagna section (<14.78 Ma based on bio-magnetostratigraphy by Hohenegger et al. 2009; Fig. 9).

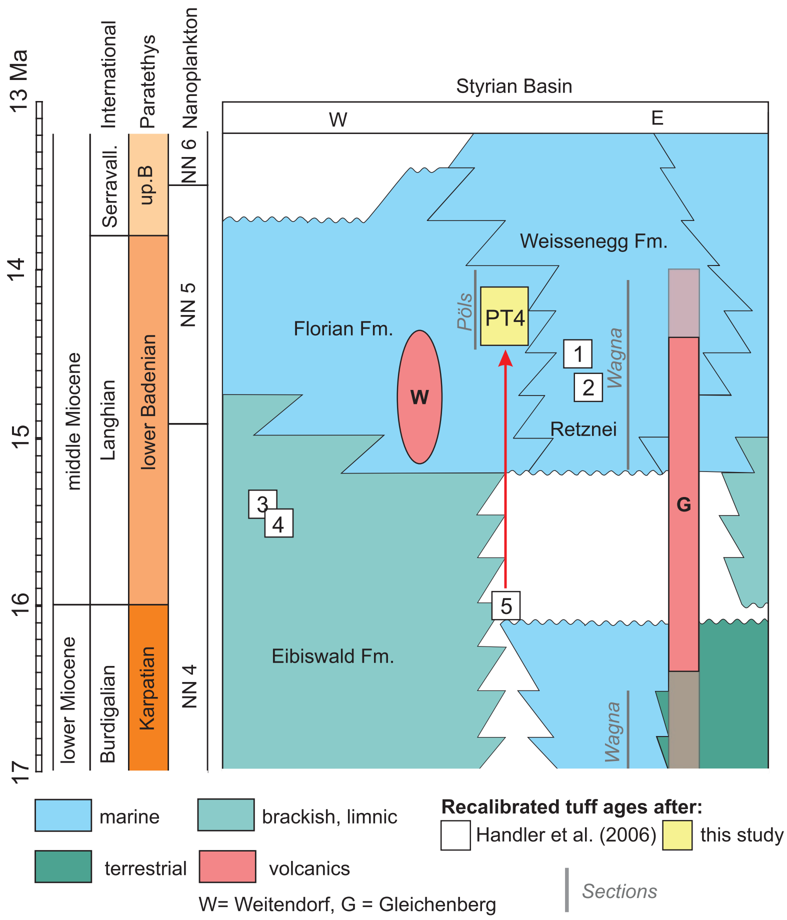

Fig. 9. Updated stratigraphy of the Styrian Basin based on the new result for the Quellgraben in Pöls (modified after Handler et al. 2006, Hohenegger et al. 2009 and Reuter et al. 2012). Note the recalibrated ages of Handler et al. (2006; Table 1). The red arrow is pointing to the shift from the original age (HA-5) towards the new age (PT4).

The Badenian flooding of the northern Vienna Basin

In the Vienna Basin an angular unconformity occurs between the Karpatian and Badenian deposits. This unconformity is linked with a hiatus dated to the early/middle Miocene boundary (hiatus base ~15.97 Ma, hiatus top ~14.90 Ma; Kováč et al. 2004; Strauss et al. 2006; Harzhauser et al. 2017, 2018 and 2019). Subsequently the Badenian marine flooding follows. The base of the marine Badenian stage in the northern Vienna Basin is difficult to detect and it seems to be associated with a disturbed and reworked interval including at least one large hiatus (Rögl et al. 2002; Ćorić & Rögl 2004; Harzhauser et al. 2018). For instance, in the Bernhardsthal wells, the Badenian flooding is documented only from the Berhardsthal-4 well, but is missing in all other wells (Harzhauser et al. 2018). The scattered occurrence and disturbed character might be related to a tectonic reorganization linked with the middle Miocene opening of the Vienna Basin, postdating the classic Styrian tectonic phase. The onset of the pull-apart mechanism or oblique extension could have been a major factor for the erosion of lowermost Badenian deposits (Kováč et al. 2004; Strauss et al. 2006). The full age range of the sample (14.85±0.29 Ma to 16.33±0.96 Ma) is in agreement with its stratigraphic position between the Ottnangian (upper Burdigalian; ~18.2–17.2 Ma) and Badenian marine strata with *Orbulina suturalis* (<14.6 Ma; Aziz et al. 2008). The majority of the $^{40}Ar/^{39}Ar$ dated grains fall in the age range of ~15–16 Ma, suggesting that the deposition of tuffite (depth 2295–2300 m) together with surrounding sediments of the Bernhardsthal-4 took place during the Langhian (Fig. 10). The older grains might represent reworked material from the basin margins.

The analysed tuffite age correlates with the age of the Kuchyňa tuff from the Slovak part of the Vienna Basin, which was dated by the same laboratory (Rybár et al. 2019). The mean weighted sanidine age of Kuchyňa tuff is

15.23±0.04 Ma (n=3), with the full range of the reliable sanidine grains from15.22±0.02 Ma to 15.40±0.01 Ma. During the Kuchyňa tuff deposition, this marginal part of the Vienna Basin was terrestrial and covered by a humid, subtropical, evergreen forest. In Bernhardsthal-4, coastal depositional settings were identified above the tuffite layer (in the depth of 2134–2141 m; Harzhauser et al., 2018). Based on this claim it can be deduced, that the Badenian flooding in the Vienna Basin started after 15.2 Ma.

Late Badenian volcanism in the Danube Basin

In the south-east Danube basin, the middle Miocene deposition starts at the lower/middle Miocene unconformity (Fig. 11). The lower Badenian andesite conglomerates of Burda Formation from the lower part of the dated section (Fig. 5a,c) are linked with the Börzsöny–Visegrád volcanic region (e.g., Bezák et al. 2009). Based on K–Ar dating and paleomagnetic data, it was concluded that the volcanic activity in the Börzsöny–Visegrád volcanic region ceased ~13.6 Ma (Karátson 1995; Karátson et al. 2000). The new $^{40}Ar/^{39}Ar$ age, however, clearly indicates that the KH2 tuff layer represents a younger volcanic event. In the Börzsöny–Visegrád volcanic region, amphibole andesite tuffs of the same age are also documented (12.5–12.6 Ma, dated by K/Ar; Karátson et al. 2000, 2007). This indicates: 1) that the KH2 tuff is widely spatially distributed; 2) the volcanic activity in the Börzsöny–Visegrád–Burda continued up to 12.6 Ma, or the KH2 tuff has its provenance in a different volcanic centre (e.g., Štiavnica Stratovolcano, which had its explosive activity at the same time ~12.7–12.2 Ma; Konečný et al. 1995; Chernyshev et al. 2013).

In the Central Paratethys region, the Badenian–Sarmatian boundary is generally connected with the BSEE (Badenian–Sarmatian extinction event) which is linked to a major drop of sea level dated to ~12.6 Ma (Harzhauser & Piller 2007; Piller et al. 2007; Paulissen et al. 2011; Mandic et al. 2019). In the Danube and Vienna Basin, this sea level fall is documented by transition from a marine environment to coastal and freshwater swamps or by similar swallowing upwards trends (Rybár et al. 2016; Ruman et al. 2017; Harzhauser et al. 2018).

The mean weighted age for the Kamenica nad Hronom section is 12.56±0.10 Ma and thus corresponds to the Badenian–Sarmatian boundary (~12.6 Ma; Paulissen et al. 2011; Mandic et al. 2019). Moreover, in this area a transition to a terrestrial environment was discussed (Seneš et al. 1962; Vaškovský et al. 1982; Nováková et al. in press). Presence of a shallow marine late Badenian environment is documented by a mollusc assemblage from the stratigraphically underlying fossiliferous sandstones occurring in the Kamenica nad Hronom shooting gallery section (Fig. 5b,d; Seneš et al. 1962; Vaškovský et al. 1982; Nováková et al. in press), the same section also includes the NN6 calcareous nannofossil biozone (~13.65–11.9 Ma) determined on a partially preserved sample containing *Discoaster*? *exilis* and lacking *Sphenolithus heteromorphus*, (Nováková et al. in press). Presence of a marine environment in the dated Kamenica nad Hronom section (Fig. 5a,c) is documented only by poriferan spicules in the lapilli tuff/tuff breccia. These tuffs are overlain by gravel, muds and coarse tuffs (KH2). These sediments are interpreted as terrestrial, based on presence of alluvial sediments together with the absence of marine fossils, and also by the presence of leaves occurring at the top of the dated coarse tuff. The fossil leaves (*Daphnogene polymorpha*, *Laurophyllum* sp. *Ternstroemites* sp.) indicate presence of broadleaved forest at the time of the coarse tuff deposition (Nováková et al in press). Thus, these sections strongly support a sea level fall via transition to a terrestrial environment at the Badenian–Sarmatian boundary.

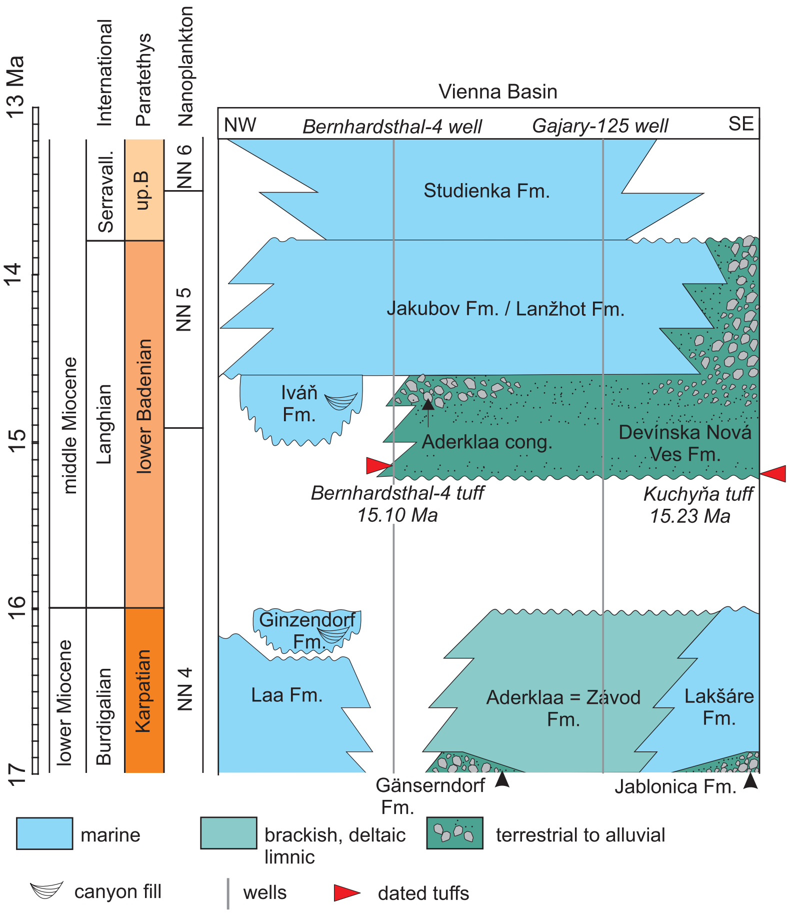

Fig. 10. Updated stratigraphy of the Vienna Basin (modified after Sauer et al. 1992; Vass 2002; Kováč et al. 2004; Harzhauser et al. 2018, 2019).

Conclusions and recommendations

The improved analytical precision of the ARGUS mass spectrometer allowed for single grain measurements on relatively small grains (~90–500 μm), which resulted in a better insight into the age distribution within tuff samples allowing a more transparent representation of the age. Comparison of single and multiple grain data of the same tuffs confirmed that $^{40}Ar/^{39}Ar$ ages based on multiple grain fusions do not necessarily reflect the youngest ages in a sample, and so could lead to a (slight) overestimation of the eruption age. $^{40}Ar/^{39}Ar$ dating on multiple grain measurements should therefore always be based on a large number of measurements (>20) in order to get a representative age determination of a tuff. A large number of single grain measurements on the same sample should be performed, so that grains affected by Ar gain or loss, or a non-uniform age in the tuff, related to magma chamber processes, can be detected (e.g., Andersen et al. 2017). Only in this case the most representative eruption age can be derived. Utilizing the highly sensitive mass spectrometer Argus VI+ provides new Ar/Ar ages for the Badenian intervals in the Danube (KH2), Vienna (BE4) and Styrian (PT4) basins that are all significantly younger than previously assumed. This study highlights the need for modern radio-isotopic age determinations for locations where no other independent chronostratigraphic controls exist. Especially for isolated sections with very limited stratigraphic constraints, the use of various dating techniques (Ar/Ar and U/Pb) is preferred to compare their outcomes. These efforts could significantly improve the stratigraphic correlations in the Paratethys which are in many regions still based on regional (bio)stratigraphy, magnetostratigraphy and correlations to 3rd order sea level fluctuations (Haq et al. 1988; Hardenbol et al. 1998; Kováč et al. 2004; Piller et al. 2007).

Lithostratigraphic summary of the dated samples:

- In the Quellgraben section of the Styrian basin, the multiple and single grain sanidine datasets from PT4 tuff have a similar age range. The maximum age range based on analytically reliable samples is 13.9–15.0 Ma, but the geological age is presumably close to the mean weighted ages of 14.31±0.27 Ma and 14.03±0.04 Ma of the single and multiple grain data, respectively. The new age agrees with the biostratigraphic data from the region (Retznei, Wagna) suggesting a mid-Langhian age (<15.3 Ma) for the Badenian flooding in the Styrian Basin.
- The $^{40}Ar/^{39}Ar$ results on a biotite-sample (BE4) from the Bernhardsthal-4 well in the Vienna Basin reveal a wide age range (~14.6–17.2 Ma). The weighted mean age based on single grain measurements (15.12±0.19 Ma) significantly differs from that based on the multiple grain dataset (15.80±0.07 Ma). The age range in the tuffite agrees with the stratigraphic position between Ottnangian and Badenian the strata are best correlated with the 15.2 Ma old Kuchyňa tuff (Rybár et al. 2019). This indicates that the Badenian flooding of the Vienna Basin took place after 15.2 Ma.
- Despite relatively low $^{40}Ar^*$ percentages, the Kamenica nad Hronom tuff (KH2; hornblende) from the Danube Basin (Želiezovce depression) yields an analytically reliable weighted mean age of 12.56±0.10 Ma. This corresponds to the Badenian–Sarmatian boundary (~12.6 Ma; Paulissen et al. 2011; Mandic et al. 2019) and underlines the expected transition from a marine to a terrestrial environment connected with a sea level lowstand.

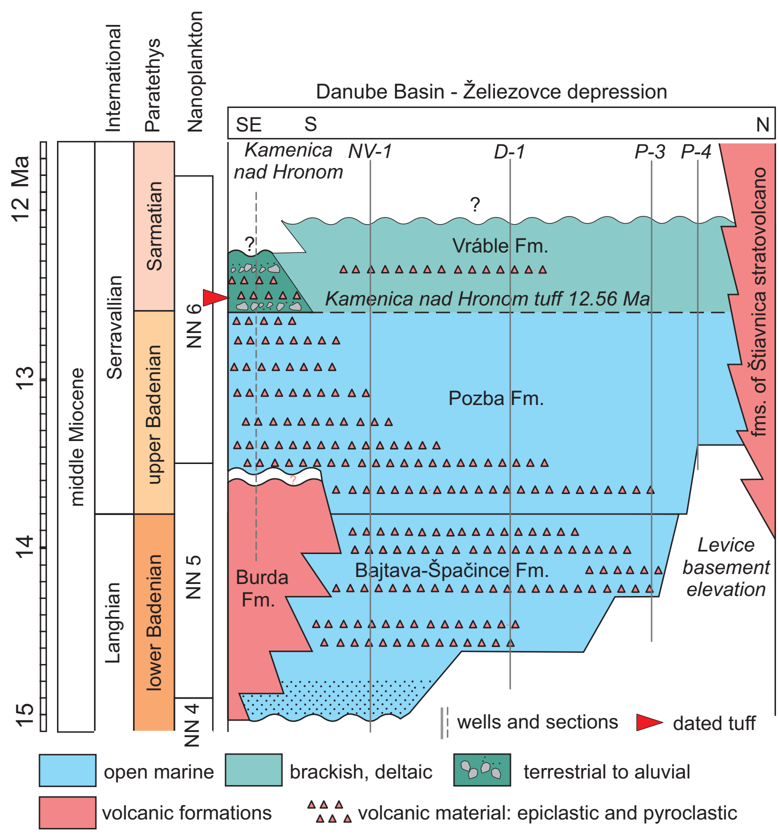

Fig. 11. Lithostratigraphic chart of the Danube Basin (Želiezovce depression) with position of the dated tuff (Vass 2002, modified after Kováč et al. 2018; Nováková et al. in press); NV-1, D-1, P-3 and P-4 — represent deep wells (Kováč et al. 2018).

Acknowledgements: Our thanks go to the team of the OMV Exploration & Production working group, and especially to Philipp Strauss, for cooperation. Special thanks go to Roel van Elsas and Lara Borst for their support in the mineral separation laboratory at the VU University, and to Michal Kováč and the whole 'Tiger Team' (Tomáš, Tamás, Andrea and Andrej) for their support with the Slovak field-work. This research was financially supported through the Netherlands Geosciences Foundation (ALW) with funding from the Netherlands Organization for Scientific Research (NWO) by VICI grant 865.10.011 of WK, and by the Slovak Research and Development Agency with the projects APVV-15-0575 and APVV-16-0121. Special thanks go to the Editors and Reviewers for guidance and insightful comments.

References

Abdul Aziz H., Di Stefano A., Foresi L.M., Hilgen F.J., Iaccarino S.M., Kuiper K.F., Lirer,F., Salvatorini G. & Turco E. 2008: Integrated stratigraphy and 40 Ar / 39 Ar chronology of early Middle Miocene sediments from DSDP Leg 42A , Site 372 (Western Mediterranean). *Palaeogeogr. Palaeoclimatol. Palaeoecol.* 257, 123–138. https://doi.org/10.1029/2004PA001129

Andersen N.L., Jicha B.R., Singer B.S. & Hildreth W. 2017: Incremental heating of Bishop Tuff sanidine reveals preeruptive radiogenic Ar and rapid remobilization from cold storage. *Proc. Natl. Acad. Sci*. 201709581. https://doi.org/10.1073/pnas.1709581114

Balogh K., Mihaliková A. & Vass D. 1981: K/Ar dating of the youngest calc-alkali rocks in the Central Slovakia field. *Západ. Karpaty, Ser. Geol*. 7, 113–126.

Balogh K., Ebner F. & Ravasz C. 1994: K/Ar-Alter tertiärer Vulkanite der südöstlichen Steiermark und des südlichen. Burgenlandes. *Jubil. 20 Jahre Geol. Zusammenarbeit Österreich* 2, 55–72.

Balogh K., Konečný V. & Lexa J. 1998: K/Ar dating of the youngest calc-alkali rocks in the Central Slovakia field. In: K/Ar Dating of the Youngest Calc-Alkali Rocks in the Central Slovakia Field. Vienna, 1–59.

Bezák V. (ed), Biely A., Broska I., Bóna J., Buček S., Elečko M., Filo I., Fordinál K., Gazdačko Ľ., Grecula P., Hraško Ľ., Ivanička J., Jacko S. sen., Jacko S. jun., Janoško J., Kaličiak M., Kobulský J., Kohút M., Konečný V., Kováčik M., Kováčik M., Lexa J., Madarás J., Maglay J., Mello J., Nagy A., Németh Z., Olšavský M., Plašienka D., Polák M., Potfaj M., Pristaš J., Siman P., Šimon L., Teťák F., Vozárová A., Vozár J. & Žec B. 2009: Explanatory notes to the general geological map of the Slovak Republic 1:200 000. *ŠGÚDŠ*, Bratislava, 1–534 (in Slovak with English summary).

Bukowski K., Sant K., Pilarz M., Kuiper K. & Garecka M. 2018: Radio-isotopic age and biostratigraphic position of a lower Badenian tuffite from the western Polish Carpathian Foredeep Basin (Cieszyn area). *Geol. Quarterly* 62. https://doi.org/10.7306/gq.1402

Çelik Ö.F., Marzoli A., Marschik R., Chiaradia M., Neubauer F. & Öz I. 2011: Early-Middle Jurassic intra-oceanic subduction in the Izmir-Ankara-Erzincan Ocean, Northern Turkey. *Tectonophysics* 509, 120–134. https://doi.org/10.1016/j.tecto.2011.06.007

Chernyshev I.V., Konečný V., Lexa J., Kovalenker V.A., Jeleň S., Lebedev V.A. & Goltsman Y.V. 2013: K–Ar and Rb–Sr geochronology and evolution of the Štiavnica Stratovolcano (Central Slovakia). *Geol. Carpath.* 64, 327–351. https://doi.org/10.2478/geoca-2013-0023

Ćorić S. & Rögl F. 2004: Roggendorf-1 borehole, a keysection for Lower Badenian transgressions and the stratigraphic position of the Grund Formation (Molasse Basin, Lower Austria). *Geol. Carpath.* 55, 165–178.

Daşçi H.T., Parlak O., Nurlu N. & Billor Z. 2015: Geochemical characteristics and age of metamorphic sole rocks within a Neotethyan ophiolitic mélange from Konya region (central southern Turkey). *Geodin. Acta* 27, 223–243. https://doi.org/10.1080/09853111.2014.979532

de Leeuw A., Bukowski K., Krijgsman W. & Kuiper K.F. 2010: Age of the Badenian salinity crisis; Impact of Miocene climate variability on the circum-mediterranean region. *Geology* 38, 715–718. https://doi.org/10.1130/G30982.1

de Leeuw A., Filipescu S., Maţenco L., Krijgsman W., Kuiper K. & Stoica M. 2013: Paleomagnetic and chronostratigraphic constraints on the Middle to Late Miocene evolution of the Transylvanian Basin (Romania): Implications for Central Paratethys stratigraphy and emplacement of the Tisza–Dacia plate. *Glob. Planet. Change* 103, 82–98. https://doi.org/10.1016/j.gloplacha.2012.04.008

de Leeuw A., Tulbure M., Kuiper K.F., Melinte-Dobrinescu M.C., Stoica M. & Krijgsman W. 2018: New $^{40}Ar/^{39}Ar$, magnetostratigraphic and biostratigraphic constraints on the termination of the Badenian Salinity Crisis: Evidence for tectonic improvement of basin interconnectivity in Southern Europe. *Glob. Planet. Change* 169, 1–15. https://doi.org/10.1016/j.gloplacha.2018.07.001

Dilek Y., Thy P., Bradley H. & Sidsel G. 1999: Structure and petrology of Tauride ophiolites and mafic dike intrusions (Turkey): Implications for the Neotethyan ocean. *GSA Bull*. 111, 1192–1216. https://doi.org/10.1130/0016-7606(1999)111<1192:SAPOTO>2.3.CO;2

Ebner F. & Gräf W. 1977: The fauna of Weitendorf.Jber. Landesmus. *Joanneum Graz 1976* N. F 6, 157–183 (in German).

Ebner F. & Sachsenhofer R.F. 1995: Palaeogeography, subsidence and thermal history of the Neogene Styrian Basin (Pannonian basin system, Austria). *Tectonophysics* 242, 133–150. https://doi.org/10.1016/0040-1951(94)00155-3

Handler R., Ebner F., Neubauer F., Bojar A. & Hermann S. 2006: $^{40}Ar/^{39}Ar$ dating of Miocene tuffs from the Styrian part of the Pannonian Basin : an attempt to refine the basin stratigraphy. *Geol. Carpath.* 57, 483–494.

Haq B.U., Hardenbol J. & Vail P.R. 1988: Mesozoic and Cenozoic chronostratigraphy and cycles of sea level changes. In: Wilgus C.K. (Ed.): Sea-Level Changes — an Integrated Approach. *Society of Economic Paleontologists and Mineralogists, Spec. Publ.* 42, 71–108.

Harangi Sz. & Lenkey L. 2007: Genesis of the Neogene to Quaternary volcanism in the Carpathian-Pannonian region: Role of subduction, extension, and mantle plume. In: Beccaluva L., Bianchini G. & Wilson M. (Eds.): Cenozoic Volcanism in the Mediterranean Area: *Geol. Soc. Am., Spec. Pap.* 418, 67–92.

Hardenbol J., Thierry J., Farley M.B., Jacquin T., de Graciansky P. & Vail P.R. 1998: Mesozoic and Cenozoic sequence chronostratigraphic framework of European basins. *SEPM Spec. Publ*. 60, 3–13.

Harzhauser M. & Piller W.E. 2007: Benchmark data of a changing sea — Palaeogeography, Palaeobiogeography and events in the Central Paratethys during the Miocene. *Palaeogeogr. Palaeoclimatol. Palaeoecol*. 253, 8–31. https://doi.org/0.1016/j.palaeo.2007.03.031

Harzhauser M., Theobalt D., Strauss P., Mandic O., Carnevale G. & Piller W.E. 2017: Miocene biostratigraphy and paleoecology of the Mistelbach Halfgraben in the northwestern Vienna Basin (Lower Austria). *Jahrb. Geol. Bundesanst.* 157, 57–108.

Harzhauser M., Grunert P., Mandic O., Lukeneder P., Gallardo Á.G., Neubauer T.A., Carnevale G., Landau B.M., Sauer R. & Strauss P. 2018: Middle and late Badenian palaeoenvironments in the northern Vienna Basin and their potential link to the Badenian Salinity Crisis. *Geol. Carpath.* 69, 149–168. https://doi.org/10.1515/geoca-2018-0009

Harzhauser M., Theobalt D., Strauss P., Mandic O. & Piller W.E. 2019: Seismic-based lower and middle Miocene stratigraphy in the northwestern Vienna Basin (Austria). *Newslett. Stratigr.* 52, 2, 221–247.

Hilgen F.J., Lourens L.J. & Van Dam J.A. 2012: The Neogene Period. In: The Geologic Time Scale 2012, Volume 2, 923–978.

Hohenegger J., Rögl F., Ćorić S., Pervesler P., Lirer F., Roetzel R., Scholger R. & Stingl K. 2009: The Styrian Basin: A key to the Middle Miocene (Badenian/Langhian) Central Paratethys transgressions. *Austrian J. Earth Sci*. 102, 102–132.

Hohenegger J., Ćorić S. & Wagreich M. 2014: Timing of the Middle Miocene Badenian Stage of the Central Paratethys. *Geol. Carpath.* 65, 55–66. https://doi.org/10.2478/geoca-2014-0004

Hora J.M., Singer B.S., Jicha B.R., Beard B.L., Johnson C.M., de Silva S. & Salisbury M. 2010: Volcanic biotite-sanidine $^{40}Ar/^{39}Ar$ age discordances reflect Ar partitioning and pre-eruption closure in biotite. *Geology* 38, 923–926. https://doi.org/10.1130/G31064.1

Horváth F., Bada G., Szafián P., Tari G., Ádám A. & Cloetingh S. 2006: Formation and deformation of the Pannonian Basin: constraints from observational data. *Geol. Soc. London, Mem*. 32, 191–206. https://doi.org/10.1144/GSL.MEM.2006.032.01.11

Karátson D. 1995: Ignimbrite formation, resurgent doming and dome collapse activity in the Miocene Börzsöny Mountains, North Hungary. *Acta Volcanol*. 7, 107–117.

Karátson D., Márton E., Harangi S., Józsa S., Balogh K., Pécskay Z., Kovácsvölgyi S., Szakmány G. & Dulai A. 2000: Volcanic evolution and stratigraphy of the Miocene Börzsony Mountains, Hungary: An integrated study. *Geol. Carpath.* 51, 325–343.

Karátson D., Oláh I., Pécskay Z., Márton E., Harangi S., Dulai A., Zelenka T. & Kósik S. 2007: Miocene volcanism in the Visegrád Mountains (Hungary): an integrated approach to regional volcanic stratigraphy. *Geol. Carpath.* 58, 6, 541–563.

Kollmann K. 1965: Early Tertiary in the Styrian Basin. *Mitteilungen der Geol. Gesellschaft Wien* 57, 479–632 (in German).

Konečný V., Lexa J. & Hojstričová V. 1995: The Central Slovakia Neogene volcanic field: a review. *Acta Volcanol*. 7, 63–78.

Kopetzky G. 1957: The Miocene between Kainach and Laßnitz in south-western Steiermark.*Mitt. Mus. Bergbau, Geol. Techn* 18, 1–112 (in German).

Koppers A.A.P. 2002: ArArCALC F software for $^{40}Ar/^{39}Ar$ age calculations. *Comput. Geosci*. 28, 605–619.

Kováč M., Baráth I., Harzhauser M., Hlavatý I. & Hudáčková N. 2004: Miocene depositional systems and sequence stratigraphy of the Vienna Basin Depositional systems and sequence stratigraphy. *Cour. Forsch.-Inst. Senckenberg* 246, 187–212.

Kováč M., Andreyeva-Grigorovich A., Bajraktarević Z., Brzobohatý R., Filipescu S., Fodor L., Harzhauser M., Nagymarosy A., Oszczypko N., Pavelić D., Rögl F., Saftić B., Sliva U. & Studencka B. 2007: Badenian evolution of the Central Paratethys Sea: paleogeography, climate and eustatic sea-level changes. *Geol. Carpath.* 58, 579–606.

Kováč M., Márton E., Oszczypko N., Vojtko R., Hók J., Králiková S., Plašienka D., Klučiar T., Hudáčková N. & Oszczypko-Clowes M. 2017: Neogene palaeogeography and basin evolution of the Western Carpathians, Northern Pannonian domain and adjoining areas. *Glob. Planet. Change* 155, 133–154. https://doi.org/10.1016/j.gloplacha.2017.07.004

Kováč M., Rybár S., Halásová E., Hudáčková N., Šarinová K., Šujan M., Baranyi V., Kováčová M., Ruman A., Klučiar T. & Zlinská A. 2018: Changes in Cenozoic depositional environment and sediment provenance in the Danube Basin. *Basin Res*. 97–131. https://doi.org/10.1111/bre.12244

Kuiper K.F., Deino A., Hilgen F.J., Krijgsman W., Renne P.R. & Wijbrans J.R. 2008: Synchronizing rock clocks of Earth history. *Science* 320, 500–504. https://doi.org/10.1126/science.1154339

Lee J.Y., Marti K., Severinghaus J.P., Kawamura K., Yoo H.S., Lee J.B. & Kim J.S. 2006: A redetermination of the isotopic abundances of atmospheric Ar. *Geochim. Cosmochim. Acta* 70, 4507–4512. https://doi.org10.1016/j.gca.2006.06.1563

Lexa J., Seghedi I., Németh K., Szakács A., Konečný V., Pécskay Z., Fülöp A. & Kovacs M. 2010: Neogene-Quaternary Volcanic forms in the Carpathian-Pannonian Region: a review. *Cent. Eur. J. Geosci*. 2, 3, 207–270.

Lukács R., Harangi S., Guillong M., Bachmann O., Fodor L., Buret Y., Dunkl I., Sliwinski J., von Quadt A., Peytcheva I. & Zimmerer M. 2018: Early to Mid-Miocene syn-extensional massive silicic volcanism in the Pannonian Basin (East-Central Europe): Eruption chronology, correlation potential and geodynamic implications. *Earth-Sci. Rev*. 179, 1–19. https://doi.org/10.1016/j.earscirev.2018.02.005

Mandic O., de Leeuw A., Bulić J., Kuiper K.F., Krijgsman W. & Jurišić-Polšak Z. 2012: Paleogeographic evolution of the Southern Pannonian Basin: $^{40}Ar/^{39}Ar$ age constraints on the Miocene continental series of Northern Croatia. *Int. J. Earth Sci*. 101, 1033–1046. https://doi.org/10.1007/s00531-011-0695-6

Mandic O., Sant K., Kallanxhi M-E., Ćorić S., Theobalt D., Grunert P., de Leeuw A. & Krijgsman W. 2019: Integrated bio-magnetostratigraphy of the Badenian reference section Ugljevik in southern Pannonian Basin — implications for the Paratethys history (middle Miocene, Central Europe). *Glob. Planet. Change* 172, 374–395.

McDougall I. & Harrison T.M. 1999: Geochronology and Thermochronology by the $^{40}Ar/^{39}Ar$ Method, 2. ed. *Oxford University Press*, New York.

Min K., Mundil R., Renne P.R. & Ludwig K.R. 2000: A test for systematic errors in $^{40}Ar/^{39}Ar$ geochronology through comparison with U/Pb analysis of a 1.1-Ga rhyolite. *Geochim. Cosmochim. Acta* 64, 73–98. https://doi.org/10.1016/S0016-7037(99)00204-5

Nebert K. 1989: The Neogene between Sulm and Laßnitz (southwestern Steiermark). *Jahrb. Geol. Bundesanst.* 132, 727–743 (in German).

Nováková P., Rybár S., Šarinová K., Nagy A., Hudáčková N., Jamrich M., Teodoridis V., Kováčová M., Šujan M., Vlček T. & Kováč M. 2020:: The late Badenian-Sarmatian (Serravallian) environmental transition calibrated by sequence stratigraphy (Eastern Danube Basin, Central Paratethys). *Geol. Carpath.*, in press.

Onstott T.C., Miller M.L., Ewing R.C., Arnold G.W. & Walsh D.S. 1995: Recoil refinements: Implications for the $^{40}Ar/^{39}Ar$ dating technique. *Geochim. Cosmochim. Acta* 59, 1821–1834.

Palcu D. V., Golovina L.A., Vernyhorova Y. V., Popov S.V. & Krijgsman W. 2017: Middle Miocene paleoenvironmental crises in Central Eurasia caused by changes in marine gateway configuration. *Glob. Planet. Change* 158, 57–71. https://doi.org/10.1016/j.gloplacha.2017.09.013

Palcu D.V., Tulbure M., Bartol M., Kouwenhoven T.J. & Krijgsman W. 2015: The Badenian–Sarmatian Extinction Event in the Carpathian foredeep basin of Romania: Paleogeographic changes in the Paratethys domain. *Glob. Planet. Change* 133, 346–358. https://doi.org/10.1016/j.gloplacha.2015.08.014

Papp A., Cicha I. & Seneš J. 1978: Gliederung des Badenien Faunenzonen und Unterstufen. In: Papp A., Cicha I., Senes J. & Steininger F. (Eds.): M4, Badenian (Moravian, Wielician, Kosovian). Chronostratigraphy and neostratotypes, Miocene of the Central Paratethys. *VEDA*, Bratislava, 49–52 (in German).

Parlak O., Karaoglan F., Rizaoglu T., Klötzli U., Koller F. & Billor Z. 2013: U–Pb and $^{40}Ar–^{39}Ar$ geochronology of the ophiolites and granitoids from the Tauride belt: Implications for the evolution of the Inner Tauride suture. *J. Geodyn*. 65, 22–37. https://doi.org/10.1016/j.jog.2012.06.012

Paulissen W.E., Luthi S.M., Grunert P., Ćorić S. & Harzhauser M. 2011: Integrated high-resolution stratigraphy of a Middle to Late Miocene sedimentary sequence in the central part of the Vienna Basin *Geol. Carpath.* 62, 2, 155–169. https://doi.org/10.2478/v10096-011-0013-z

Pécskay Z., Lexa J., Szakács A., Seghedi I., Balogh K., Konečný V., Zelenka T., Kovacs M., Póka T., Fülöp A., Márton E., Panaiotu C. & Cvetković V. 2006: Geochronology of Neogene magmatism in the Carpathian arc and intra-Carpathian area. *Geol. Carpath.* 57, 511–530.

Phillips D. & Matchan E.L. 2013: Ultra-high precision $^{40}Ar/^{39}Ar$ ages for Fish Canyon Tuff and Alder Creek Rhyolite sanidine: New dating standards required? *Geochim. Cosmochim. Acta* 121, 229–239. https://doi.org/10.1016/j.gca.2013.07.003

Piller W.E., Egger H., Erhart C., Gross M., Harzhauser M., Hubmann B., van Husen D., Krenmayr H.-G., Krystyn L., Lein R., Lukeneder A., Mandl G., Rögl F., Roetzel R., Rupp C., Schnabel W., Schönlaub H.P., Summesberger H. & Wagreich M. 2004: Die Stratigraphische Tabelle von Österreich 2004 (sedimentäre Schichtfolgen). *Österreichische Stratigraphische Komission*

Piller W.E., Harzhauser M. & Mandic O. 2007: Miocene Central Paratethys stratigraphy — current status and future directions. *Stratigraphy* 4, 151–168.

Popov S.V., Rögl F., Rozanov A.Y., Steininger F.F., Shcherba I.G. & Kovac M. 2004: Lithological-paleogeographic maps of Paratethys. In: CFS Courier Forschungsinstitut Senckenberg. 1–46.

Popov S.V., Antipov M.P., Zastrozhnov A.S., Kurina E.E. & Pinchuk T.N. 2010: Sea-level fluctuations on the northern shelf of the Eastern Paratethys in the Oligocene-Neogene. *Stratigr. Geol. Correl*. 18, 200–224. https://doi.org/10.1134/S0869593810020073

Renne P.R., Swisher C.C., Deino A.L., Karner D.B., Owens T.L. & DePaolo D.J. 1998: Intercalibration of standards, absolute ages and uncertainties in $^{40}Ar/^{39}Ar$ dating. *Chem. Geol*. 145, 117–152. https://doi.org/10.1016/S0009-2541(97)00159-9

Renne P.R., Balco G., Ludwig K.R., Mundil R. & Min K. 2011: Response to the comment by W.H. Schwarz, on "Joint determination of ^{40}K decay constants and $^{40}Ar^*/^{40}K$ for the Fish Canyon sanidine standard, and improved accuracy for $^{40}Ar/^{39}Ar$ geochronology" by Renne et al. (2010). *Geochim Cosmochim Acta* 75, 5097–5100.

Reuter M., Piller W.E. & Erhart C. 2012: A Middle Miocene carbonate platform under silici-volcaniclastic sedimentation stress (Leitha Limestone, Styrian Basin, Austria) — Depositional environments, sedimentary evolution and palaeoecology. *Palaeogeogr. Palaeoclimatol. Palaeoecol.* 350–352, 198–211. https://doi.org/10.1016/j.palaeo.2012.06.032

Rocholl A., Schaltegger U., Gilg H.A., Wijbrans J. & Böhme M. 2017: The age of volcanic tuffs from the Upper Freshwater Molasse (North Alpine Foreland Basin) and their possible use for tephrostratigraphic correlations across Europe for the Middle Miocene. *Int. J. Earth Sci*. 107, 387–407. https://doi.org/10.1007/s00531-017-1499-0

Rögl F. 1998: Palaeogeographic Considerations for Mediterranean and Paratethys Seaways (Oligocene to Miocene). *Ann. des Naturhistorischen Museums Wien* 99A, 279–310.

Rögl F., Spezzaferri S. & Ćorić S. 2002: Micropaleontology and biostratigraphy of the Karpatian-Badenian transition (Early-Middle Miocene boundary) in Austria (Central Paratethys). *Cour. Forschungsinst. Senckenb.* 47–67.

Ruman A., Rybár S., Hudáčková N., Šujan M. & Halásová E. 2017: Depositional environment changes at the Early–Late Serravallian boundary dated by the Central Paratethys bioevents. *Facies* 63, 9, 1–13. https://doi.org/10.1007/s10347-016-0490-8

Rybár S., Kováč M., Šarinová K., Halásová E., Hudáčková N., Šujan M., Kováčová M., Ruman A. & Klučiar T. 2016: Neogene changes in paleeogeography, palaeoenvironment and the provenance of sediment in the Northern Danube Basin. *Bull. Geosci.* 91, 2, 367–398. https://doi.org/10.3140/bull.geosci.1571

Rybár S., Šarinová K., Sant K., Kuiper K.F., Kováčová M., Vojtko R., Reiser M.K., Fordinál K., Teodoridis V., Nováková P. & Vlček T. 2019: New $^{40}Ar/^{39}Ar$, fission track and sedimentological data on a middle Miocene tuff occurring in the Vienna Basin: Implications for the north-western Central Paratethys region. *Geol. Carpath.* 70, 5, 386–404. https://doi.org/10.2478/geoca-2019-0022

Sant K., Palcu D.V., Mandic O. & Krijgsman W. 2017: Changing seas in the Early–Middle Miocene of Central Europe: a Mediterranean approach to Paratethyan stratigraphy. *Terra Nov*a 29, 273–281. https://doi.org/10.1111/ter.12273

Sant K., Palcu D.V., Turco E., Di Stefano A., Baldassini N., Kouwenhoven T., Kuiper K.F. & Krijgsman W. 2019: The mid-Langhian flooding in the eastern Central Paratethys: integrated stratigraphic data from the Transylvanian Basin and SE Carpathian Foredeep. *IJES* 108, 2209–2232. https://doi.org/10.1007/s00531-019-01757-z

Sauer R., Seifert P. & Wessely G. 1992: Part I: Outline of Sedimentation,Tectonic Framework and Hydrocarbon Occurrence in Eastern Lower Austria. In: Guidebook to Excursions in the Vienna Basin and the adjacent Alpine–Carpathian thrustbelt in Austria. *Mitt. Österr. Geol. Ges*. 85, 5–96.

Seneš J., Franko O., Koštálik J. & Porubský A. 1962: Explanations for the geological map 1:200 000, Nové Zámky sheat L-34-1. *ŠGÚDŠ*, 1–151.

Schreilechner M.G. & Sachsenhofer R.F. 2007: High Resolution Sequence Stratigraphy in the Eastern Styrian Basin (Miocene, Austria). *Austrian J. Earth Sci*. 100, 164–184.

Spezzaferri S., Ćorić S. & Stingl K. 2009: Palaeoenvironmental reconstruction of the Karpatian-Badenian (Late Burdigalian–Early Langhian) transition in the Central Paratethys. A case study from the Wagna section (Austria). *Acta Geol. Pol*. 4, 523–544.

Steiger R.H. & Jäger E. 1977: Subcommission on geochronology: convention on the use of decay constants in geo- and cosmochronology. *Earth Planet. Sci. Lett.* 36, 359–362.

Strauss P., Harzhauser M., Hinsch R. & Wagreich M. 2006: Sequence stratigraphy in a classic pull-apart basin (Neogene , Vienna Basin). A 3D seismic based integrated approach. *Geol. Carpath.* 57, 185–197.

Tari G., Dovenyi P., Dunkl I., Horvath F., Lenkey L., Stefanescu M., Szafian P. & Toth T. 1999: Lithospheric structure of the Pannonian basin derived from seismic, gravity and geothermal data. *Geol. Soc. London, Spec. Publ*. 156, 215–250. https://doi.org/10.1144/GSL.SP.1999.156.01.12

Turner G. & Cadogan P.H. 1974: Possible effects of ^{39}Ar recoil in ^{40}Ar–^{39}Ar dating. *Proc. Fifth Lunar Sci. Conf.* 2, 1601–1615.

Vass D. 2002: Lithostratigraphy of Western Carpathians: Neogene and Buda Paleogene. *Štátny geologický ústav Dionýza Štúra*, Bratislava, 1–202 (in Slovak).

Vaškovský I., Bárta R., Hanzel V., Halouzka R., Harčár J., Karolus K., Pristaš J., Remšík A., Šucha P., Vass D. & Vškovská E. 1982: Explanation for the geological map of southeaster part od the Danube Basin. 1:500 000. *ŠGÚDŠ*, 1–115.

Wijbrans J.R., Pringle M.S., Koppers A.A.P. & Scheveers R. 1995: Argon geochronology of small samples using the Vulkaan argon laserprobe. *Proc. Kon. Nederl. Akad. Wetensch* 98, 185–218.

Appendix

Representative analyses of K-feldspars, altered grains and clays. Chemical composition of K-feldspar was calculated based on 8 oxygens. *FeO recalculated to Fe_2O_3.

	K-feldspar							**altered grains**		**clay**		
analyse	**1**	**5**	**6**	**8**	**9**	**11**	**7**	**12**	**14**		**3**	**10**
grain	**1**	**2**	**3**	**5**	**6**	**7**	**4**	**2**	**4**			
Formula	**sanidine**	**sanidine**	**sanidine**	**sanidine**	**sanidine**	**sanidine**	**orthoclase**					
SiO_2	64.30	65.51	63.34	65.41	65.16	63.57	66.58	75.63	70.38	SiO_2	60.78	63.79
Al_2O_3	19.84	19.96	19.69	19.91	20.32	20.21	18.84	13.11	15.19	TiO_2	0.08	0.07
FeO	0.14	0.12	0.12	0.11	0.14	0.16	0.12	0.16	0.12	Al_2O_3	18.56	19.47
MgO	0.00	0.00	0.07	0.00	0.00	0.00	0.04	0.02	0.01	Cr_2O_3	0.00	0.02
BaO	1.97	1.46	1.46	0.66	0.93	1.73	0.03	0.02	0.11	Fe_2O_3*	2.76	3.01
CaO	0.17	0.18	0.46	0.17	0.21	0.17	0.07	0.37	0.30	MgO	5.17	5.89
Na_2O	3.30	3.40	3.22	3.34	3.49	3.43	0.40	2.27	2.84	MnO	0.10	0.12
K_2O	11.05	11.31	11.17	11.56	11.30	11.12	14.73	7.32	8.15	NiO	0.03	0.00
Total	*100.77*	*101.94*	*99.54*	*101.17*	*101.54*	*100.40*	*100.82*	*98.90*	*97.11*	CaO	2.44	2.14
Si	2.940	2.949	2.929	2.954	2.936	2.918	3.018			K_2O	0.17	0.10
Al	1.069	1.059	1.073	1.060	1.079	1.093	1.006			Na_2O	0.07	0.06
Fe	0.005	0.004	0.005	0.004	0.005	0.006	0.005			Cl	0.05	0.05
Mg	0.000	0.000	0.005	0.000	0.000	0.000	0.003			F	0.00	0.00
Ba	0.035	0.026	0.026	0.012	0.016	0.031	0.001			*Total*	*89.92*	*94.41*
Ca	0.009	0.009	0.023	0.008	0.010	0.008	0.003					
Na	0.293	0.297	0.289	0.293	0.305	0.305	0.035					
K	0.644	0.650	0.659	0.666	0.650	0.651	0.852					
cat sum	*4.994*	*4.994*	*5.009*	*4.996*	*5.001*	*5.013*	*4.922*					
Orthoclase	68.15	68.00	67.88	68.88	67.38	67.50	95.67					
Albite (%)	30.95	31.09	29.77	30.27	31.59	31.64	3.95					
Anorthite	0.90	0.90	2.35	0.85	1.04	0.87	0.38					

Supplement A

Background information about Ar–Ar sample preparation

The samples PT1, PT4, BE4 and KH2 were crushed into ~1 cm^3 blocks, disintegrated in a diluted calgon solution with a Robot Coupe blixer 4 v.v., treated in an ultrasonic bath, and wet sieved into a fraction between 90 and 500 µm.

K-feldspar (sanidine) was separated from sample PT4. The K-feldspar grains were isolated from the 2.54–2.59 g/cm^3 density fraction (using di-iodomethane), cleaned in an ultrasonic water bath and dry sieved again over a 90 µm sieve. The separate was purified by magnetic separation over the Frantz isodynamic separator. The 90–200 µm size fraction contained sanidine from which the most transparent sanidine grains were handpicked under an optical microscope.

Biotite was extracted from the density fraction >3.00 g/cm^3 from samples BE4 and PT4 by heavy liquid separation (using di-iodomethane). Sample BE4 was dry sieved (>125 µm), cleaned in an ultrasonic bath, magnetically purified over the Frantz isodynamic separator (Fr >500 mA), again cleaned in an ultrasonic bath, and finally sieved into the fractions 200–250 µm and 250–500 µm. The separate from PT4 was very pure after the heavy liquid separation, so was cleaned by an ultrasonic bath in water and dry sieved into the fractions 90–150, 150–200 and 200–400 µm. The thickest, most angular hexagonal biotite minerals without inclusions as visible under an optical microscope were handpicked from both samples for radio-isotopic dating.

Finally, heavy liquid separation was used to isolate hornblende from the density fraction 3.06–3.3 g/cm3 in sample KH2. The separate was subsequently leached by a 10 minute ultrasonic HNO_3 bath for cleaning, rinsed with distilled water and dry sieved over 300 and 400 µm. Clean hornblende grains were handpicked under an optical microscope (fraction 400–500 µm) for radio-isotopic dating.

Supplement B

Analytical data of all Ar–Ar measurements (samples PT4, BE4, KH2)

A) PT4: Quellgraben section in Pöls

PT4 — sample K12b: multiple grain, size fraction: 90–200 μm

Age result PT4 (sanidine)	40(a)/36(a)	± 2σ	40(r)/39(k)	± 2σ	Age (Ma)	± 2σ	MSWD	N	K/Ca	± 2σ
Weighted mean age			1.64349	± 0.00514	14.03	± 0.04	2.00	27.00	21.7	± 16.9
				± 0.31 %		± 0.32 %	11 %	4		
					External error	± 0.30	2.63	2σ Confidence Limit		
					Analytical Error	± 0.04	1.4142	*Error Magnification*		
Normal Isochron	312.54	± 39.07	1.63789	± 0.01674	13.98	± 0.14	1.97	27.00		
		± 12.50 %		± 1.02 %		± 1.02 %	14 %	4		
					External error	± 0.33	3.00	2σ Confidence Limit		
					Analytical Error	± 0.14	1.4034	*Error Magnification*		
						1		*Number of Iterations*		
						0.0000097672		*Convergence*		
Inverse Isochron	319.91	± 37.06	1.63480	± 0.01588	13.96	± 0.14	1.73	27.00		
		± 11.58 %		± 0.97 %		± 0.97 %	18 %	4		
					External error	± 0.32	3.00	2σ Confidence Limit		
					Analytical Error	± 0.14	1.3161	*Error Magnification*		
						3		*Number of Iterations*		
						0.0000466634		*Convergence*		
						6 %		*Spreading Factor*		

PT4 — sample K12: single grain, size fraction: 90–200 μm

Age result PT4 (sanidine)	40(a)/36(a)	± 2σ	40(r)/39(k)	± 2σ	Age (Ma)	± 2σ	MSWD	N	K/Ca	± 2σ
Weighted mean age			1.67651	± 0.03153	14.31	± 0.27	0.34	16.29	0.5	± 3.6
				± 1.88 %		± 1.87 %	79 %	4		
					External error	± 0.40	2.63	2σ Confidence Limit		
					Analytical Error	± 0.27	1.0000	*Error Magnification*		
Normal Isochron	315.29	± 43.62	1.65172	± 0.06369	14.10	± 0.54	0.00	12.96		
		± 13.84 %		± 3.86 %		± 3.84 %	94 %	3		
					External error	± 0.62	3.83	2σ Confidence Limit		
					Analytical Error	± 0.54	1.0000	*Error Magnification*		
						1		*Number of Iterations*		
						0.0000097672		*Convergence*		
Inverse Isochron	314.70	± 42.69	1.65280	± 0.06149	14.11	± 0.52	0.00	12.96		
		± 13.57 %		± 3.72 %		± 3.71 %	95 %	3		
					External error	± 0.60	3.83	2σ Confidence Limit		
					Analytical Error	± 0.52	1.0000	*Error Magnification*		
						2		*Number of Iterations*		
						0.0000491031		*Convergence*		
						27 %		*Spreading Factor*		

PT4 — sample K12b [K12_combined]: multiple grain, size fraction: 90–200 μm

Negative values in red

Relative abundances	Selected for mean age calc.	36Ar [fA]	%1σ	37Ar [fA]	%1σ	38Ar [fA]	%1σ	39Ar [fA]	%1σ	40Ar [fA]	%1σ	40(r)/39 (k) ± 2σ	Age ± 2σ	40Ar(r)	39Ar(k)	K/Ca ± 2σ
103_VU109-K12_COMBINED	x	0.0098036	2.495	0.0384182	612.274	0.2231453	2.764	23.02115	0.086	40.6437	0.075	1.63736 ± 0.00761	13.98 ± 0.06	92.74	6.44	257.7 ± 3155.3
108_VU109-K12_COMBINED	x	0.0050415	3.892	0.0045698	4485.377	0.2289339	2.651	22.56654	0.091	38.5643	0.062	1.64134 ± 0.00653	14.01 ± 0.06	96.05	6.31	2123.4 ± 190485.0
106_VU109-K12_COMBINED	x	0.0105561	2.369	0.4811549	42.802	0.2378919	2.584	22.79055	0.087	40.6658	0.074	1.64687 ± 0.00776	14.06 ± 0.07	92.29	6.37	20.4 ± 17.4
102_VU109-K12_COMBINED	x	0.0164363	1.783	0.2995204	81.158	0.2871285	2.482	28.16678	0.089	51.3538	0.063	1.64898 ± 0.00739	14.08 ± 0.06	90.44	7.88	40.4 ± 65.6
100_VU109-K12_COMBINED		0.0409870	0.797	0.6312437	36.030	0.5285068	1.052	51.66231	0.085	97.6152	0.072	1.65274 ± 0.00550	14.11 ± 0.05	87.47	14.45	35.2 ± 25.4
099_VU109-K12_COMBINED		0.0276742	1.171	0.2846230	84.065	0.2723940	2.886	25.63329	0.091	50.8031	0.114	1.65962 ± 0.00946	14.17 ± 0.08	83.74	7.17	38.7 ± 65.1
105_VU109-K12_COMBINED		0.0063988	4.041	0.2055895	106.397	0.1002130	7.062	9.49858	0.109	17.7214	0.107	1.66543 ± 0.01751	14.22 ± 0.15	89.26	2.66	19.9 ± 42.3
087_VU109-K12_COMBINED		0.0088666	2.952	0.1130315	221.776	0.1616397	3.820	13.45619	0.103	25.1252	0.129	1.67026 ± 0.01337	14.26 ± 0.11	89.45	3.76	51.2 ± 227.1
097_VU109-K12_COMBINED		0.0877091	0.565	0.7322016	32.883	0.3480212	1.640	30.86770	0.091	78.5625	0.083	1.69783 ± 0.01114	14.49 ± 0.09	66.71	8.63	18.1 ± 11.9
091_VU109-K12_COMBINED		0.0626291	0.598	0.3662295	62.966	0.1934779	3.505	18.82452	0.094	51.0257	0.118	1.71798 ± 0.01414	14.67 ± 0.12	63.38	5.26	22.1 ± 27.8
096_VU109-K12_COMBINED		0.0697911	0.605	0.0677687	312.768	0.1555795	4.613	13.64187	0.096	44.4953	0.094	1.73379 ± 0.02015	14.80 ± 0.17	53.16	3.82	86.6 ± 541.5
093_VU109-K12_COMBINED		0.1414692	0.446	0.2922570	86.467	0.2162213	3.062	22.20109	0.091	81.5389	0.069	1.76836 ± 0.01853	15.09 ± 0.16	48.15	6.21	32.7 ± 56.5
088_VU109-K12_COMBINED		0.2496717	0.450	0.5445059	35.970	0.2947304	1.915	21.92658	0.095	116.1659	0.088	1.89946 ± 0.03299	16.21 ± 0.28	35.85	6.13	17.3 ± 12.5
090_VU109-K12_COMBINED		0.3752974	0.398	0.2056128	103.530	0.3180275	2.151	25.10765	0.089	160.6432	0.088	1.93524 ± 0.03858	16.51 ± 0.33	30.25	7.02	52.5 ± 108.7
094_VU109-K12_COMBINED		0.4651192	0.379	0.2542188	100.915	0.3629582	1.577	28.17941	0.088	194.3156	0.040	1.96760 ± 0.03931	16.79 ± 0.33	28.53	7.88	47.7 ± 96.2
	Σ	**1.5774509**	**0.181**	**3.8504554**	**23.053**	**3.9288693**	**0.639**	**357.54421**	**0.025**	**1089.2396**	**0.023**					

PT4 — sample K12: single grain, size fraction: 90–200 μm

Relative abundances		36Ar [fA]	%1σ	37Ar [fA]	%1σ	38Ar [fA]	%1σ	39Ar [fA]	%1σ	40Ar [fA]	%1σ	40(r)/39 (k) ± 2σ	Age ± 2σ	40Ar(r)	39Ar(k)	K/Ca ± 2σ
174_VU109-K12		0.0041182	9.861	0.1542203	413.812	0.0034096	124.923	0.01626	43.124	1.19663	1.494	2.73826 ± 16.35888	23.62 ± 142.03	3.75	0.01	0.0 ± 0.4
145_VU109-K12		0.0254617	2.225	0.6186552	91.234	0.0374580	18.923	2.19862	0.288	11.24310	0.190	1.63309 ± 0.16067	13.94 ± 1.37	31.94	1.85	1.5 ± 2.8
131_VU109-K12		0.0258488	1.683	0.3145111	157.796	0.0565812	13.094	3.05152	0.178	12.75787	0.135	1.64319 ± 0.08996	14.03 ± 0.77	39.31	2.56	4.2 ± 13.2
162_VU109-K12	x	0.0002625	186.540	0.7194050	85.522	0.0505422	11.623	4.46753	0.173	7.36021	0.213	1.65130 ± 0.06955	14.10 ± 0.59	100.24	3.75	2.7 ± 4.6
170_VU109-K12		0.0153786	3.769	1.5917273	37.071	0.0801885	6.526	6.33375	0.096	15.19727	0.144	1.65355 ± 0.05710	14.12 ± 0.49	68.93	5.32	1.7 ± 1.3
133_VU109-K12	x	0.0009374	58.704	0.4725634	135.827	0.0349708	24.762	3.59949	0.223	6.21736	0.285	1.65917 ± 0.09632	14.17 ± 0.82	96.05	3.02	3.3 ± 8.9
141_VU109-K12		0.0211072	2.315	1.5583654	39.235	0.0762117	9.355	6.50831	0.104	17.31827	0.084	1.67268 ± 0.04759	14.28 ± 0.40	62.87	5.47	1.8 ± 1.4
149_VU109-K12		0.0021322	29.755	1.3752881	53.795	0.0620733	11.248	5.63897	0.124	10.21240	0.188	1.67779 ± 0.07073	14.32 ± 0.60	92.66	4.74	1.8 ± 1.9
168_VU109-K12		0.0000137	4499.485	1.2036127	54.572	0.0617912	11.854	5.52249	0.174	9.37190	0.213	1.67802 ± 0.06980	14.33 ± 0.59	98.89	4.64	2.0 ± 2.2
139_VU109-K12		0.0144298	3.515	0.2158278	361.952	0.0391373	19.181	3.83197	0.176	10.73547	0.155	1.68093 ± 0.08599	14.35 ± 0.73	60.00	3.22	7.6 ± 55.3
176_VU109-K12	x	0.0137826	4.033	0.2333100	198.985	0.0961716	5.069	7.36239	0.106	16.49152	0.094	1.68279 ± 0.04651	14.37 ± 0.40	75.12	6.18	13.6 ± 54.0
172_VU109-K12		0.0835129	0.627	0.6863537	94.275	0.1169050	6.142	8.34623	0.080	39.08399	0.057	1.68799 ± 0.04037	14.41 ± 0.34	36.05	7.01	5.2 ± 9.9
184_VU109-K12	x	0.0036983	10.674	0.5233485	127.109	0.0379291	21.786	3.96452	0.209	5.57610	0.309	1.69471 ± 0.06604	14.47 ± 0.56	120.48	3.33	3.3 ± 8.3
164_VU109-K12		0.0169310	4.091	0.4159521	156.957	0.1049374	7.158	8.15641	0.085	18.92778	0.107	1.69596 ± 0.05259	14.48 ± 0.45	73.09	6.85	8.4 ± 26.5
178_VU109-K12		0.0290933	1.591	0.8944037	80.416	0.0472087	14.379	3.32336	0.261	14.27625	0.116	1.70279 ± 0.09108	14.54 ± 0.77	39.63	2.79	1.6 ± 2.6
135_VU109-K12		0.0426792	1.621	0.4607687	116.724	0.0518876	17.025	4.65742	0.125	20.88634	0.078	1.75567 ± 0.09111	14.99 ± 0.77	39.15	3.91	4.3 ± 10.1
143_VU109-K12		0.0097398	6.390	0.7850104	89.883	0.0279458	21.503	2.87009	0.204	8.01634	0.247	1.75714 ± 0.13605	15.00 ± 1.16	62.92	2.41	1.6 ± 2.8
127_VU109-K12		0.0027788	16.229	0.2956264	196.275	0.0910291	6.397	6.82381	0.101	11.17602	0.149	1.76212 ± 0.04211	15.04 ± 0.36	107.59	5.73	9.9 ± 39.0
147_VU109-K12		0.0062834	7.986	0.6467317	116.159	0.0503956	11.347	3.98796	0.204	5.18432	0.336	1.78261 ± 0.08160	15.21 ± 0.69	137.11	3.35	2.7 ± 6.2
182_VU109-K12		0.0111149	4.454	0.9988937	79.513	0.1314195	5.531	9.63105	0.093	20.53144	0.099	1.79482 ± 0.03377	15.32 ± 0.29	84.19	8.09	4.1 ± 6.6
166_VU109-K12		0.3939077	0.378	0.2371119	262.878	0.1066001	4.857	2.92727	0.263	123.13537	0.018	1.88188 ± 0.31757	16.06 ± 2.70	4.47	2.46	5.3 ± 27.9
160_VU109-K12		0.0509619	1.000	1.9796642	36.213	0.0370010	16.796	3.00681	0.253	20.99298	0.099	1.97348 ± 0.10985	16.84 ± 0.93	28.25	2.52	0.7 ± 0.5
180_VU109-K12		0.0852307	1.163	1.7065515	38.441	0.1038621	4.981	7.17641	0.089	74.06282	0.025	6.75379 ± 0.08509	56.99 ± 0.71	65.45	6.03	1.8 ± 1.4
137_VU109-K12		0.0164315	3.293	1.0619517	49.172	0.0489952	15.872	5.63261	0.119	67.38575	0.027	11.10796 ± 0.06522	92.81 ± 0.53	92.84	4.73	2.3 ± 2.2
129_VU109-K12		0.0016921	28.706	0.2089614	284.439	0.0080137	106.176	0.01484	48.708	0.11029	17.160	27.99347 ± 34.59974	225.45 ± 262.18	372.99	0.01	0.0 ± 0.2
	Σ	**0.8480979**	**0.370**	**3.3747135**	**95.431**	**1.5466379**	**2.216**	**119.05009**	**0.031**	**547.22720**	**0.017**					

PT4 — K2, single grain biotite, size fraction 200–400

Negative values in red

Relative abundances	**36Ar [fA]**	**%1σ**	**37Ar [fA]**	**%1σ**	**38Ar [fA]**	**%1σ**	**39Ar [fA]**	**%1σ**	**40Ar [fA]**	**%1σ**	**40(r)/39 (k) ± 2σ**	**Age ± 2σ**	**40Ar(r)**	**39Ar(k)**	**K/Ca ± 2σ**
186_VU107-K2	0.0684845	1.129	0.1060394	221.228	0.0378551	22.824	1.902776	0.428	22.96650	0.036	1.32801 ± 0.24478	11.10 ± 2.04	11.00	5.04	7.7 ± 34.1
191_VU107-K2	0.0215826	4.447	0.3532506	97.118	0.1008777	13.846	5.344954	0.204	15.42785	0.125	1.67574 ± 0.10818	14.00 ± 0.90	58.06	14.17	6.5 ± 12.6
183_VU107-K2	0.0205512	2.030	0.2680964	93.373	0.1250774	8.134	8.246679	0.150	20.23196	0.055	1.71149 ± 0.03116	14.30 ± 0.26	69.76	21.86	13.2 ± 24.7
189_VU107-K2	0.0425975	1.560	0.6857729	28.610	0.1077654	7.926	6.422573	0.199	24.25979	0.054	1.80534 ± 0.06265	15.08 ± 0.52	47.79	17.02	4.0 ± 2.3
188_VU107-K2	0.0465281	1.412	0.1292551	166.976	0.2471511	4.442	15.810407	0.116	42.59409	0.040	1.81572 ± 0.02541	15.16 ± 0.21	67.40	41.91	52.6 ± 175.6
Σ	**0.1997438**	**0.802**	**0.8359132**	**67.722**	**0.6187268**	**3.848**	**37.727389**	**0.077**	**125.48019**	**0.026**					

PT4 — sample K12b [K12_combined]: multiple grain, size fraction: 90–200 µm

Negative values in red

Procedure Blanks	**36Ar [fA]**	**1σ**	**37Ar [fA]**	**1σ**	**38Ar [fA]**	**1σ**	**39Ar [fA]**	**1σ**	**40Ar [fA]**	**1σ**
103_VU109-K12_COMBINED	0.0166646	0.0001221	0.0409546	0.0002709	0.0029272	0.0047038	0.0058756	0.0048101	3.8458437	0.0073109
108_VU109-K12_COMBINED	0.0169132	0.0001564	0.0407646	0.0002320	0.0004136	0.0047600	0.0108272	0.0040222	3.7616694	0.0086332
106_VU109-K12_COMBINED	0.0166318	0.0001425	0.0402823	0.0002320	0.0032208	0.0045127	0.0026525	0.0043533	3.7833576	0.0064468
102_VU109-K12_COMBINED	0.0166646	0.0001221	0.0409546	0.0002709	0.0029272	0.0047038	0.0058756	0.0048101	3.8458437	0.0073109
100_VU109-K12_COMBINED	0.0166362	0.0001284	0.0402481	0.0002711	0.0089807	0.0040635	0.0004712	0.0034714	3.8025169	0.0098682
099_VU109-K12_COMBINED	0.0166362	0.0001284	0.0402481	0.0002711	0.0089807	0.0040635	0.0004712	0.0034714	3.8025169	0.0098682
105_VU109-K12_COMBINED	0.0166318	0.0001425	0.0402823	0.0002320	0.0032208	0.0045127	0.0026525	0.0043533	3.7833576	0.0064468
087_VU109-K12_COMBINED	0.0167982	0.0001563	0.0401694	0.0001936	0.0139196	0.0038894	0.0077182	0.0039805	3.8187038	0.0125469
097_VU109-K12_COMBINED	0.0166472	0.0002113	0.0403053	0.0002031	0.0103167	0.0050859	0.0020135	0.0048081	3.8026083	0.0058065
091_VU109-K12_COMBINED	0.0172614	0.0001777	0.0400496	0.0002017	0.0019764	0.0044969	0.0078763	0.0042382	3.8685441	0.0095694
096_VU109-K12_COMBINED	0.0166472	0.0002113	0.0403053	0.0002031	0.0103167	0.0050859	0.0020135	0.0048081	3.8026083	0.0058065
093_VU109-K12_COMBINED	0.0168962	0.0001688	0.0402308	0.0003227	0.0118392	0.0024463	0.0080041	0.0041445	3.8462179	0.0066151
088_VU109-K12_COMBINED	0.0167982	0.0001563	0.0401694	0.0001936	0.0139196	0.0038894	0.0077182	0.0039805	3.8187038	0.0125469
090_VU109-K12_COMBINED	0.0172614	0.0001777	0.0400496	0.0002017	0.0019764	0.0044969	0.0078763	0.0042382	3.8685441	0.0095694
094_VU109-K12_COMBINED	0.0168962	0.0001688	0.0402308	0.0003227	0.0118392	0.0024463	0.0080041	0.0041445	3.8462179	0.0066151

Sample Parameters	**Material**	**Standard (Ma)**	**%1σ**	**J**	**%1σ**	**MDF**	**%1σ**	**Day**	**Time**
103_VU109-K12_COMBINED	sanidine	28.201	0.08	0.00468	0.03	0.994843	0.08	16jan18	1:43
108_VU109-K12_COMBINED	sanidine	28.201	0.08	0.00468	0.03	0.994843	0.08	16jan18	4:32
106_VU109-K12_COMBINED	sanidine	28.201	0.08	0.00468	0.03	0.994843	0.08	16jan18	3:25
102_VU109-K12_COMBINED	sanidine	28.201	0.08	0.00468	0.03	0.994843	0.08	16jan18	1:09
100_VU109-K12_COMBINED	sanidine	28.201	0.08	0.00468	0.03	0.994843	0.08	16jan18	0:02
099_VU109-K12_COMBINED	sanidine	28.201	0.08	0.00468	0.03	0.994843	0.08	15jan18	23:27
105_VU109-K12_COMBINED	sanidine	28.201	0.08	0.00468	0.03	0.994843	0.08	16jan18	2:50
087_VU109-K12_COMBINED	sanidine	28.201	0.08	0.00468	0.03	0.994843	0.08	15jan18	16:40
097_VU109-K12_COMBINED	sanidine	28.201	0.08	0.00468	0.03	0.994843	0.08	15jan18	22:20
091_VU109-K12_COMBINED	sanidine	28.201	0.08	0.00468	0.03	0.994843	0.08	15jan18	18:57
096_VU109-K12_COMBINED	sanidine	28.201	0.08	0.00468	0.03	0.994843	0.08	15jan18	21:46
093_VU109-K12_COMBINED	sanidine	28.201	0.08	0.00468	0.03	0.994843	0.08	15jan18	20:03
088_VU109-K12_COMBINED	sanidine	28.201	0.08	0.00468	0.03	0.994843	0.08	15jan18	17:16
090_VU109-K12_COMBINED	sanidine	28.201	0.08	0.00468	0.03	0.994843	0.08	15jan18	18:23
094_VU109-K12_COMBINED	sanidine	28.201	0.08	0.00468	0.03	0.994843	0.08	15jan18	20:39

PT4 — sample K12: single grain, size fraction: 90–200 µm

Negative values in red

Procedure Blanks	36Ar [fA]	1σ	37Ar [fA]	1σ	38Ar [fA]	1σ	39Ar [fA]	1σ	40Ar [fA]	1σ
174_VU109-K12	0.0449593	0.0002171	0.0763560	0.0050939	0.0056344	0.0028439	0.0854767	0.0047576	10.558348	0.013916
145_VU109-K12	0.0418440	0.0002804	0.0575808	0.0041870	0.0071498	0.0043876	0.0950948	0.0038441	9.441482	0.013094
131_VU109-K12	0.0424133	0.0002941	0.0610450	0.0038875	0.0054021	0.0043317	0.1025193	0.0027343	9.567707	0.014003
162_VU109-K12	0.0561584	0.0002810	0.0635333	0.0037318	0.0029775	0.0038183	0.1043060	0.0038510	14.506558	0.010875
170_VU109-K12	0.0464623	0.0002682	0.0727577	0.0044677	0.0031539	0.0035866	0.1016730	0.0039311	11.143942	0.010353
133_VU109-K12	0.0565444	0.0002849	0.0598097	0.0063860	0.0076776	0.0060331	0.0984485	0.0052023	14.661036	0.009844
141_VU109-K12	0.0407878	0.0003105	0.0732565	0.0034891	0.0000648	0.0045695	0.1080777	0.0047633	9.122888	0.010827
149_VU109-K12	0.0419095	0.0003714	0.0684180	0.0071197	0.0058081	0.0037450	0.0970060	0.0032722	9.464925	0.014303
168_VU109-K12	0.0485927	0.0002529	0.0710565	0.0051398	0.0025781	0.0046738	0.0952506	0.0038767	11.885019	0.011989
139_VU109-K12	0.0447374	0.0003007	0.0637431	0.0064558	0.0059820	0.0045462	0.1053066	0.0039505	10.471530	0.007136
176_VU109-K12	0.0471312	0.0003123	0.0629938	0.0048132	0.0000470	0.0033866	0.1017192	0.0046079	11.457604	0.011494
172_VU109-K12	0.0469748	0.0002340	0.0527018	0.0054539	0.0028741	0.0041214	0.1041894	0.0031197	11.447251	0.012776
184_VU109-K12	0.0505047	0.0002554	0.0552234	0.0060819	0.0018623	0.0055438	0.0955429	0.0040400	12.740295	0.010135
164_VU109-K12	0.0439643	0.0003446	0.0707851	0.0042056	0.0013049	0.0030715	0.0960106	0.0045262	10.141997	0.012935
178_VU109-K12	0.0471312	0.0003123	0.0629938	0.0048132	0.0000470	0.0033866	0.1017192	0.0046079	11.457604	0.011494
135_VU109-K12	0.0439001	0.0003295	0.0618635	0.0038800	0.0078396	0.0044533	0.1028546	0.0045425	9.989249	0.010819
143_VU109-K12	0.0450292	0.0004000	0.0710719	0.0058313	0.0014995	0.0032741	0.1047913	0.0040253	10.347169	0.012295
127_VU109-K12	0.0511059	0.0002663	0.0590441	0.0048899	0.0032372	0.0040178	0.1044148	0.0041518	12.403867	0.010318
147_VU109-K12	0.0601474	0.0002606	0.0592760	0.0057653	0.0020428	0.0029692	0.0970039	0.0051565	15.596149	0.012164
182_VU109-K12	0.0446824	0.0002253	0.0619793	0.0085134	0.0017618	0.0056069	0.1214271	0.0044114	10.312770	0.013724
166_VU109-K12	0.0452571	0.0002831	0.0615055	0.0062985	0.0013757	0.0031192	0.1053360	0.0041006	10.698274	0.012774
160_VU109-K12	0.0464387	0.0002606	0.0466882	0.0050993	0.0029285	0.0031248	0.0978758	0.0048823	10.882498	0.014545
180_VU109-K12	0.0455012	0.0003620	0.0793182	0.0050060	0.0045408	0.0033091	0.0840377	0.0042312	10.847482	0.008874
137_VU109-K12	0.0439001	0.0003295	0.0618635	0.0038800	0.0078396	0.0044533	0.1028546	0.0045425	9.989249	0.010819
129_VU109-K12	0.0511059	0.0002663	0.0590441	0.0048899	0.0032372	0.0040178	0.1044148	0.0041518	12.403867	0.010318

Sample Parameters	Material	Standard (Ma)	%1σ	J	%1σ	MDF	%1σ	Day	Time
174_VU109-K12	sanidine	28.201	0.08	0.00468	0.03	0.96387	0.02	28sep17	23:45
145_VU109-K12	sanidine	28.201	0.08	0.00468	0.03	0.96387	0.02	28sep17	14:20
131_VU109-K12	sanidine	28.201	0.08	0.00468	0.03	0.96387	0.02	28sep17	9:58
162_VU109-K12	sanidine	28.201	0.08	0.00468	0.03	0.96387	0.02	28sep17	20:00
170_VU109-K12	sanidine	28.201	0.08	0.00468	0.03	0.96387	0.02	28sep17	22:30
133_VU109-K12	sanidine	28.201	0.08	0.00468	0.03	0.96387	0.02	28sep17	10:35
141_VU109-K12	sanidine	28.201	0.08	0.00468	0.03	0.96387	0.02	28sep17	13:05
149_VU109-K12	sanidine	28.201	0.08	0.00468	0.03	0.96387	0.02	28sep17	15:35
168_VU109-K12	sanidine	28.201	0.08	0.00468	0.03	0.96387	0.02	28sep17	21:53
139_VU109-K12	sanidine	28.201	0.08	0.00468	0.03	0.96387	0.02	28sep17	12:28
176_VU109-K12	sanidine	28.201	0.08	0.00468	0.03	0.96387	0.02	29sep17	0:23
172_VU109-K12	sanidine	28.201	0.08	0.00468	0.03	0.96387	0.02	28sep17	23:08
184_VU109-K12	sanidine	28.201	0.08	0.00468	0.03	0.96387	0.02	29sep17	2:52
164_VU109-K12	sanidine	28.201	0.08	0.00468	0.03	0.96387	0.02	28sep17	20:38
178_VU109-K12	sanidine	28.201	0.08	0.00468	0.03	0.96387	0.02	29sep17	1:00
135_VU109-K12	sanidine	28.201	0.08	0.00468	0.03	0.96387	0.02	28sep17	11:13
143_VU109-K12	sanidine	28.201	0.08	0.00468	0.03	0.96387	0.02	28sep17	13:43
127_VU109-K12	sanidine	28.201	0.08	0.00468	0.03	0.96387	0.02	28sep17	8:43
147_VU109-K12	sanidine	28.201	0.08	0.00468	0.03	0.96387	0.02	28sep17	14:57
182_VU109-K12	sanidine	28.201	0.08	0.00468	0.03	0.96387	0.02	29sep17	2:15
166_VU109-K12	sanidine	28.201	0.08	0.00468	0.03	0.96387	0.02	28sep17	21:15
160_VU109-K12	sanidine	28.201	0.08	0.00468	0.03	0.96387	0.02	28sep17	19:23
180_VU109-K12	sanidine	28.201	0.08	0.00468	0.03	0.96387	0.02	29sep17	1:37
137_VU109-K12	sanidine	28.201	0.08	0.00468	0.03	0.96387	0.02	28sep17	11:50
129_VU109-K12	sanidine	28.201	0.08	0.00468	0.03	0.96387	0.02	28sep17	9:20

PT4 — K2, single grain biotite, size fraction 200–400

Negative values in red

Procedure Blanks	36Ar [fA]	1σ	37Ar [fA]	1σ	38Ar [fA]	1σ	39Ar [fA]	1σ	40Ar [fA]	1σ
186_VU107-K2	0.0402202	0.0004231	0.0111093	0.0001394	0.0868925	0.0052174	0.1095156	0.0038780	8.0581995	0.0055727
191_VU107-K2	0.0484057	0.0008002	0.0117240	0.0002990	0.0967286	0.0123756	0.1041384	0.0072414	10.6365832	0.0166215
183_VU107-K2	0.0439041	0.0002879	0.0109503	0.0001428	0.0983561	0.0072724	0.1294924	0.0057852	9.0293152	0.0043743
189_VU107-K2	0.0473106	0.0003791	0.0108056	0.0001100	0.0950258	0.0066465	0.1067988	0.0067867	9.7291757	0.0077164
188_VU107-K2	0.0473106	0.0003791	0.0108056	0.0001100	0.0950258	0.0066465	0.1067988	0.0067867	9.7291757	0.0077164

Sample Parameters	Material	Standard (Ma)	%1σ	J	%1σ	MDF	%1σ	Day	Time
186_VU107-K2	biotite	28.201	0.08	0.004579	0.1	0.9944	0.1	14feb17	11:52
191_VU107-K2	biotite	28.201	0.08	0.004579	0.1	0.9944	0.1	14feb17	13:38
183_VU107-K2	biotite	28.201	0.08	0.004579	0.1	0.9944	0.1	14feb17	10:56
189_VU107-K2	biotite	28.201	0.08	0.004579	0.1	0.9944	0.1	14feb17	12:52
188_VU107-K2	biotite	28.201	0.08	0.004579	0.1	0.9944	0.1	14feb17	12:31

Information on Analysis and used Constants for samples of PT4 (K12, K12b)		**Information on Analysis and used Constants for samples of PT4 (K2)**	
Analysis		***Analysis***	
Material	sanidine	Material	biotite
Location	Pöls section - Styrian Basin	Location	Pöls section - Styrian Basin
Analyst	K. Kuiper	Analyst	K. Kuiper
Project	VU109	Project	VU107
Mass Discr. Law	LIN	Mass Discr. Law	LIN
Irradiation	VU109	Irradiation	VU107
J	0.00467960 ± 0.00000140	J	0.00457860 ± 0.00000458
FCs	28.201 ± 0.023 Ma	FCs	28.201 ± 0.023 Ma
Heating	45 sec	Heating	45 sec
Isolation	3.00 min	Isolation	3.00 min
Instrument	ARGUS	Instrument	ARGUS
Constants			
Age Equations	Min et al. (2000)	*Same constants as to the left*	
Negative Intensities	Allowed		
Decay Constant 40K	5.460 ± 0.053 E-10 1/a		
Decay Constant 39Ar	2.940 ± 0.016 E-07 1/h		
Decay Constant 37Ar	8.230 ± 0.012 E-04 1/h		
Decay Constant 36Cl	2.257 ± 0.015 E-06 1/a		
Decay Activity 40K(EC,β^+)	3.310 ± 0.030 1/gs		
Decay Activity 40K(β^-)	27.890 ± 0.150 1/gs		
Atmospheric Ratio 40/36(a)	298.56 ± 0.31		
Atmospheric Ratio 38/36(a)	0.1885 ± 0.0003		
Production Ratio 39/37(ca)	0.000673 ± 0.000004		
Production Ratio 36/37(ca)	0.000264 ± 0.000002		
Production Ratio 40/39(k)	0.000860 ± 0.000070		
Production Ratio 38/39(k)	0.012110 ± 0.000030		
Production Ratio 36/38(cl)	262.80 ± 1.71		
Scaling Ratio K/Ca	0.43		
Abundance Ratio 40K/K	1.1700 ± 0.0100 E-04		
Atomic Weight K	39.0983 ± 0.0001 g		

B) BE4: Bernhardstahll 4 well, Viena Basin

BE4 —Summary of age calculation of K13b (multiple grain, size fraction 250–500 µm)

Age result BE4 (biotite)	40(a)/36(a)	± 2σ	40(r)/39(k)	± 2σ	Age (Ma)	± 2σ	MSWD	N	K/Ca	± 2σ
Weighted mean age			1.85377	± 0.00409	15.80	± 0.07	1.83	46.04	16.4	± 6.7
				± 0.22 %		± 0.43 %	8 %	8		
					External error	± 0.34	2.07	2σ Confidence Limit		
					Analytical Error	± 0.03	1.3519	*Error Magnification*		
Normal Isochron	304.66	± 12.85	1.84698	± 0.01449	15.74	± 0.14	1.93	46.04		
		± 4.22 %		± 0.78 %		± 0.87 %	7 %	8		
					External error	± 0.36	2.15	2σ Confidence Limit		
					Analytical Error	± 0.12	1.3882	*Error Magnification*		
						79		*Number of Iterations*		
							0.0000182400	*Convergence*		
Inverse Isochron	303.69	± 12.98	1.84824	± 0.01462	15.75	± 0.14	1.94	46.04		
		± 4.28 %		± 0.79 %		± 0.87 %	7 %	8		
					External error	± 0.36	2.15	2σ Confidence Limit		
					Analytical Error	± 0.12	1.3934	*Error Magnification*		
							2	*Number of Iterations*		
							0.0004757438	*Convergence*		
							13 %	*Spreading Factor*		

BE4 — K13 Single grain, size fraction 250–500 µm

Age result BE4 (biotite)	40(a)/36(a)	± 2σ	40(r)/39(k)	± 2σ	Age (Ma)	± 2σ	MSWD	N	K/Ca	± 2σ
Weighted mean age			1.77432	± 0.02137	15.12	± 0.19	1.53	21.07	2.5	± 1.9
				± 1.20 %		± 1.26 %	19 %	5		
					External error	± 0.37	2.41	2σ Confidence Limit		
					Analytical Error	± 0.18	1.2374	*Error Magnification*		
Normal Isochron	283.22	± 34.57	1.78573	± 0.03821	15.22	± 0.33	1.79	21.07		
		± 12.20 %		± 2.14 %		± 2.16 %	15 %	5		
					External error	± 0.46	2.63	2σ Confidence Limit		
					Analytical Error	± 0.32	1.3371	*Error Magnification*		
						85		*Number of Iterations*		
						0.0000177513		*Convergence*		
Inverse Isochron	287.39	± 35.49	1.78437	± 0.03881	15.21	± 0.33	1.82	21.07		
		± 12.35 %		± 2.18 %		± 2.20 %	14 %	5		
					External error	± 0.46	2.63	2σ Confidence Limit		
					Analytical Error	± 0.33	1.3483	*Error Magnification*		
						3		*Number of Iterations*		
						0.0000021531		*Convergence*		
						33 %		*Spreading Factor*		

BE4 — K13b [K13 combined] Multiple grain, size fraction 250–500 µm Negative values in red

Relative abundances	Selected for mean age calc.	36Ar [fA]	%1σ	37Ar [fA]	%1σ	38Ar [fA]	%1σ	39Ar [fA]	%1σ	40Ar [fA]	%1σ	40(r)/39 (k)	± 2σ	Age	± 2σ	40Ar(r)	39Ar(k)	K/Ca	± 2σ
119_VU109-K13_COMBINED		1.7668147	0.332	0.9906119	24.749	0.7262859	0.951	26.37814	0.084	574.4463	0.004	1.78232	± 0.13922	15.19	± 1.18	8.18	4.85	11.4	± 5.7
119_VU109-K13_COMBINED		0.0503354	0.939	0.3451091	75.578	0.5214918	1.517	42.33606	0.084	90.5539	0.067	1.78375	± 0.00794	15.20	± 0.07	83.39	7.79	52.7	± 79.7
119_VU109-K13_COMBINED		0.4498010	0.361	0.5328627	38.642	0.7315905	0.932	42.78191	0.082	212.6989	0.005	1.83331	± 0.02378	15.62	± 0.20	36.87	7.87	34.5	± 26.7
119_VU109-K13_COMBINED		0.1050716	0.518	0.7379156	33.797	0.8672863	0.830	57.45820	0.082	136.7598	0.011	1.83478	± 0.00656	15.64	± 0.06	77.09	10.57	33.5	± 22.6
119_VU109-K13_COMBINED		0.1012073	0.548	0.1721342	157.170	0.7084823	1.069	46.81164	0.082	116.2062	0.011	1.83678	± 0.00788	15.65	± 0.07	73.99	8.61	116.9	± 367.6
119_VU109-K13_COMBINED		0.3346702	0.425	0.1066975	214.907	0.5882135	1.351	36.41804	0.083	167.1269	0.012	1.84519	± 0.02424	15.73	± 0.21	40.21	6.70	146.8	± 630.8
119_VU109-K13_COMBINED	x	0.0177326	1.947	0.1478554	184.800	0.4192692	1.938	29.05483	0.083	58.9860	0.020	1.84703	± 0.00792	15.74	± 0.07	90.98	5.34	84.5	± 312.3
119_VU109-K13_COMBINED	x	0.0394159	0.920	0.8854278	23.155	0.4679680	1.587	32.57817	0.084	71.9720	0.017	1.84962	± 0.00749	15.76	± 0.06	83.72	5.99	15.8	± 7.3
119_VU109-K13_COMBINED	x	0.0250182	1.322	0.0968581	284.228	0.4186481	1.922	29.97239	0.084	62.9204	0.016	1.84974	± 0.00748	15.76	± 0.06	88.11	5.51	133.1	± 756.4
119_VU109-K13_COMBINED	x	0.0634473	0.839	0.0941214	313.610	0.7202162	0.914	48.34739	0.081	108.4677	0.013	1.85140	± 0.00736	15.78	± 0.06	82.52	8.89	220.9	± 1385.4
119_VU109-K13_COMBINED	x	0.0478369	0.805	0.6188780	45.951	0.4044419	1.922	27.09077	0.086	64.4801	0.016	1.85432	± 0.00932	15.80	± 0.08	77.91	4.98	18.8	± 17.3
119_VU109-K13_COMBINED	x	0.0177277	1.600	0.1083909	198.077	0.3107557	2.841	20.49261	0.083	43.3403	0.029	1.85667	± 0.00908	15.82	± 0.08	87.79	3.77	81.3	± 322.1
119_VU109-K13_COMBINED	x	0.0341228	0.732	0.0223477	1126.582	0.4315001	1.864	30.36707	0.084	66.6305	0.018	1.85818	± 0.00606	15.84	± 0.05	84.69	5.58	584.3	± 13165.3
119_VU109-K13_COMBINED	x	0.0356650	1.014	0.1840735	113.499	0.4919901	1.379	32.45225	0.085	71.0656	0.019	1.86178	± 0.00751	15.87	± 0.06	85.02	5.97	75.8	± 172.1
119_VU109-K13_COMBINED		0.1791714	0.471	0.3349551	67.117	0.6573449	0.963	41.26210	0.083	130.3528	0.010	1.86298	± 0.01294	15.88	± 0.11	58.97	7.59	53.0	± 71.1
	Σ	**3.2680378**	**0.198**	**5.0825282**	**18.899**	**8.4654844**	**0.344**	**543.80157**	**0.022**	**1976.0073**	**0.004**								

BE4 — K13 Single grain, size fraction 250–500 µm Negative values in red

Relative abundances		36Ar [fA]	%1σ	37Ar [fA]	%1σ	38Ar [fA]	%1σ	39Ar [fA]	%1σ	40Ar [fA]	%1σ	40(r)/39 (k)	± 2σ	Age	± 2σ	40Ar(r)	39Ar(k)	K/Ca	± 2σ
039_VU109-K13		0.0552464	1.433	1.039153	51.132	0.1811976	3.875	10.89272	0.061	34.50339	0.065	1.66045	± 0.04441	14.16	± 0.38	52.42	5.76	4.5	± 4.6
001_VU109-K13	x	0.0120244	4.236	0.715100	72.000	0.1421841	5.007	9.20923	0.088	19.69381	0.100	1.74191	± 0.03460	14.85	± 0.29	81.46	4.87	5.5	± 8.0
033_VU109-K13		0.0242097	2.236	0.237216	351.937	0.1121121	6.439	7.43365	0.088	20.26251	0.097	1.75538	± 0.04740	14.96	± 0.40	64.40	3.93	13.5	± 94.8
066_VU109-K13	x	0.0095434	4.598	1.364274	30.870	0.1177368	6.769	9.27165	0.089	19.18008	0.079	1.77232	± 0.02952	15.11	± 0.25	85.67	4.90	2.9	± 1.8
015_VU109-K13		0.1180978	0.759	0.229949	259.053	0.2103228	3.407	13.24645	0.056	58.84546	0.043	1.78131	± 0.04164	15.18	± 0.35	40.10	7.00	24.8	± 128.3
041_VU109-K13		0.0314645	1.869	0.590977	96.372	0.1121005	6.214	7.27839	0.107	22.34649	0.098	1.78547	± 0.05037	15.22	± 0.43	58.15	3.85	5.3	± 10.2
035_VU109-K13		0.0207236	1.997	0.967921	52.249	0.0974364	9.026	6.60694	0.115	18.06896	0.087	1.78600	± 0.03985	15.22	± 0.34	65.31	3.49	2.9	± 3.1
017_VU109-K13		0.0534371	1.445	1.200128	47.532	0.3061108	2.652	21.15564	0.042	53.75463	0.046	1.79066	± 0.02243	15.26	± 0.19	70.47	11.18	7.6	± 7.2
021_VU109-K13	x	0.0044770	12.619	0.208834	181.918	0.1180294	8.250	7.60523	0.100	12.29457	0.111	1.79405	± 0.04534	15.29	± 0.38	110.98	4.02	15.7	± 57.0
025_VU109-K13	x	0.0112802	5.103	0.331055	170.012	0.1439682	5.494	9.87052	0.073	21.06478	0.089	1.79497	± 0.03627	15.30	± 0.31	84.11	5.22	12.8	± 43.6
027_VU109-K13	x	0.0064310	8.758	0.225206	277.734	0.0605081	13.644	3.91359	0.188	8.97845	0.256	1.80763	± 0.09058	15.41	± 0.77	78.79	2.07	7.5	± 41.5
013_VU109-K13		0.0245055	2.031	0.804563	73.365	0.1693109	4.404	11.81227	0.081	28.81604	0.063	1.82490	± 0.02675	15.55	± 0.23	74.80	6.24	6.3	± 9.3
019_VU109-K13		0.0046047	12.484	2.602943	21.489	0.1421294	5.046	11.03999	0.090	21.34745	0.098	1.82721	± 0.03250	15.57	± 0.28	94.48	5.83	1.8	± 0.8
023_VU109-K13		0.0204943	3.003	0.033512	2405.035	0.0544365	13.287	3.87052	0.189	13.19416	0.131	1.82795	± 0.10116	15.58	± 0.86	53.62	2.05	49.7	± 2388.8
064_VU109-K13		0.0069296	6.623	0.216756	308.258	0.1079677	5.491	7.03016	0.113	14.92052	0.150	1.83000	± 0.04245	15.60	± 0.36	86.22	3.72	13.9	± 86.0
045_VU109-K13		0.0063204	7.782	0.782219	72.740	0.0432589	16.827	3.42841	0.181	8.10211	0.205	1.83024	± 0.09036	15.60	± 0.77	77.43	1.81	1.9	± 2.7
043_VU109-K13		0.0284828	1.517	0.198451	245.012	0.1629591	3.070	10.78897	0.063	28.31587	0.051	1.83425	± 0.02525	15.63	± 0.21	69.89	5.70	23.4	± 114.6
051_VU109-K13		0.0103314	4.926	0.657346	97.197	0.0845528	7.395	6.30428	0.117	14.80642	0.111	1.85025	± 0.05124	15.77	± 0.43	78.79	3.33	4.1	± 8.0
049_VU109-K13		0.0069499	6.544	1.467252	38.457	0.1078152	7.636	7.18048	0.086	15.28898	0.129	1.85605	± 0.04031	15.82	± 0.34	87.16	3.79	2.1	± 1.6
029_VU109-K13		0.1213712	0.705	0.038823	1571.153	0.0680267	10.656	2.75503	0.300	41.46541	0.056	1.89638	± 0.19169	16.16	± 1.63	12.60	1.46	30.5	± 958.9
047_VU109-K13		0.0016137	39.363	2.516982	24.619	0.1231142	5.698	9.03952	0.090	17.55971	0.152	1.91085	± 0.04387	16.28	± 0.37	98.35	4.78	1.5	± 0.8
031_VU109-K13		0.0014925	38.911	0.610332	99.818	0.0488386	15.844	3.21719	0.242	6.56443	0.309	1.91657	± 0.11295	16.33	± 0.96	93.92	1.70	2.3	± 4.5
062_VU109-K13		0.0168554	2.843	1.509979	36.838	0.0708753	10.273	3.85579	0.178	12.31027	0.164	1.91862	± 0.07870	16.35	± 0.67	60.08	2.04	1.1	± 0.8
037_VU109-K13		0.0316172	2.030	0.590678	98.025	0.0591709	11.141	2.40681	0.334	14.32940	0.113	2.01214	± 0.16500	17.14	± 1.40	33.80	1.27	1.8	± 3.4
	Σ	**0.5677307**	**0.517**	**13.060411**	**22.255**	**2.8347402**	**1.279**	**189.21249**	**0.020**	**510.51809**	**0.019**								

BE4: K14 Single grain, size fraction 200-250 µm

Negative values in red

Relative abundances	36Ar [fA]	%1σ	37Ar [fA]	%1σ	38Ar [fA]	%1σ	39Ar [fA]	%1σ	40Ar [fA]	%1σ	40(r)/39 (k)	± 2σ	Age	± 2σ	40Ar(r)	39Ar(k)	K/Ca	± 2σ
080_VU109-K14	0.0288109	1.728	0.0608011	982.210	0.0875608	8.132	5.80960	0.141	18.42593	0.103	1.68954	± 0.05437	14.42	± 0.46	53.27	3.52	41.1	± 807.1
090_VU109-K14	0.0102303	4.112	1.8967913	27.938	0.0515422	14.548	3.71344	0.243	9.53367	0.186	1.70325	± 0.07241	14.54	± 0.62	66.37	2.25	0.8	± 0.5
068_VU109-K14	0.0042382	11.769	0.4999080	128.221	0.0459722	13.975	2.55260	0.257	5.60589	0.326	1.71583	± 0.12438	14.65	± 1.06	78.12	1.54	2.2	± 5.6
119_VU109-K14	0.0424423	1.386	1.2725632	46.402	0.0574677	13.026	4.48516	0.167	20.61801	0.103	1.74816	± 0.08200	14.92	± 0.70	38.04	2.71	1.5	± 1.4
094_VU109-K14	0.0754572	1.021	1.3274656	54.808	0.1648493	5.508	10.49958	0.079	41.26250	0.044	1.77352	± 0.04558	15.14	± 0.39	45.13	6.35	3.4	± 3.7
125_VU109-K14	0.0010701	48.942	0.4309674	127.784	0.1253608	5.035	9.33421	0.080	16.46101	0.092	1.80072	± 0.03504	15.37	± 0.30	102.11	5.65	9.3	± 23.8
078_VU109-K14	0.0026124	16.041	0.3778672	191.494	0.1314604	5.836	9.57547	0.076	18.06229	0.076	1.80100	± 0.02899	15.37	± 0.25	95.48	5.79	10.9	± 41.7
098_VU109-K14	0.0142698	3.360	0.5683563	106.918	0.0811380	8.786	5.18316	0.134	13.58036	0.152	1.80636	± 0.05902	15.42	± 0.50	68.94	3.14	3.9	± 8.4
096_VU109-K14	0.0079954	7.742	0.9041164	65.796	0.0956984	5.796	6.45477	0.142	14.04599	0.108	1.81685	± 0.05950	15.51	± 0.51	83.48	3.91	3.1	± 4.0
123_VU109-K14	0.0202946	2.982	2.3342818	27.379	0.1075988	5.938	7.28114	0.086	19.11580	0.084	1.81825	± 0.05185	15.52	± 0.44	69.24	4.40	1.3	± 0.7
100_VU109-K14	0.0214160	2.632	0.8533928	65.209	0.1466553	4.308	10.72724	0.093	25.98976	0.058	1.81963	± 0.03274	15.53	± 0.28	75.11	6.49	5.4	± 7.0
074_VU109-K14	0.1293087	0.644	0.3471526	192.951	0.1005709	8.439	4.95987	0.158	47.60917	0.046	1.82020	± 0.10433	15.53	± 0.89	18.96	3.00	6.1	± 23.7
115_VU109-K14	0.0061092	9.626	1.8536364	38.701	0.0816961	10.257	5.27551	0.147	11.31521	0.143	1.82671	± 0.07042	15.59	± 0.60	85.15	3.19	1.2	± 0.9
092_VU109-K14	0.0075933	6.673	1.1073897	67.974	0.1384904	5.051	9.92571	0.097	20.32233	0.092	1.82729	± 0.03315	15.59	± 0.28	89.24	6.01	3.9	± 5.2
117_VU109-K14	0.0156718	2.750	0.7802408	78.120	0.1895981	3.652	12.69646	0.056	27.82460	0.072	1.82733	± 0.02197	15.59	± 0.19	83.38	7.68	7.0	± 10.9
072_VU109-K14	0.0282465	2.275	0.0447048	1264.272	0.0913161	6.771	7.18582	0.117	4.70016	0.479	1.82747	± 0.05541	15.60	± 0.47	279.39	4.35	69.1	± 1747.7
084_VU109-K14	0.0312598	1.759	0.6435533	59.169	0.0609362	12.717	3.59782	0.241	15.91110	0.125	1.84217	± 0.09403	15.72	± 0.80	41.65	2.18	2.4	± 2.8
086_VU109-K14	0.0152094	2.960	0.7000885	86.777	0.0671383	9.915	4.70399	0.194	13.33390	0.146	1.88048	± 0.06170	16.05	± 0.52	66.33	2.85	2.9	± 5.0
082_VU109-K14	0.0639823	0.994	1.3462590	42.896	0.0616895	13.195	4.32687	0.186	10.79413	0.176	1.89492	± 0.09140	16.17	± 0.78	75.97	2.62	1.4	± 1.2
121_VU109-K14	0.0024423	19.682	0.4995309	110.327	0.0519393	16.386	3.30934	0.158	5.61867	0.373	1.90560	± 0.09169	16.26	± 0.78	112.25	2.00	2.8	± 6.3
070_VU109-K14	0.0940651	0.688	1.4860018	34.349	0.1062081	6.405	5.96410	0.136	39.36195	0.055	1.91035	± 0.06747	16.30	± 0.57	28.94	3.61	1.7	± 1.2
088_VU109-K14	0.0042663	14.204	1.1589985	48.133	0.1164096	5.775	8.14383	0.089	17.34888	0.113	1.98467	± 0.04612	16.93	± 0.39	93.15	4.93	3.0	± 2.9
076_VU109-K14	0.0256803	1.859	0.8927516	86.828	0.0252352	25.946	2.00012	0.318	11.57191	0.173	1.98721	± 0.15713	16.95	± 1.33	34.34	1.21	1.0	± 1.7
113_VU109-K14	0.0142341	4.267	0.4068243	172.652	0.1475686	3.632	10.60968	0.090	31.70072	0.059	2.58357	± 0.03622	22.01	± 0.31	86.47	6.42	11.2	± 38.7
111_VU109-K14	0.1610004	0.510	0.8416695	70.259	0.1215437	6.760	6.94581	0.114	78.35001	0.029	4.34905	± 0.07429	36.90	± 0.62	38.56	4.20	3.5	± 5.0
Σ	**0.6364242**	**0.457**	**4.8689830**	**63.577**	**2.4556437**	**1.468**	**165.26128**	**0.024**	**516.87568**	**0.018**								

BE4 — K13b [K13_combined] Multiple grain, size fraction 250–500 µm Negative values in red

Procedure Blanks	36Ar [fA]	1σ	37Ar [fA]	1σ	38Ar [fA]	1σ	39Ar [fA]	1σ	40Ar [fA]	1σ
119_VU109-K13_COMBINED	0.0182973	0.0001745	0.0404741	0.0003309	0.0105403	0.0048820	0.0188356	0.0031360	4.1441850	0.0057389
109_VU109-K13_COMBINED	0.0169132	0.0001564	0.0407646	0.0002320	0.0004136	0.0047600	0.0108272	0.0040222	3.7616694	0.0086332
124_VU109-K13_COMBINED	0.0252545	0.0001908	0.0397489	0.0002484	0.0070381	0.0054765	0.0111121	0.0044596	5.9103582	0.0053043
122_VU109-K13_COMBINED	0.0194401	0.0002414	0.0402921	0.0002481	0.0017409	0.0057732	0.0134210	0.0031347	4.5326812	0.0033868
116_VU109-K13_COMBINED	0.0182973	0.0001745	0.0404741	0.0003309	0.0105403	0.0048820	0.0188356	0.0031360	4.1441850	0.0057389
121_VU109-K13_COMBINED	0.0194401	0.0002414	0.0402921	0.0002481	0.0017409	0.0057732	0.0134210	0.0031347	4.5326812	0.0033868
128_VU109-K13_COMBINED	0.0258794	0.0002401	0.0403968	0.0002192	0.0074780	0.0049684	0.0089134	0.0045211	6.1277551	0.0056314
125_VU109-K13_COMBINED	0.0252545	0.0001908	0.0397489	0.0002484	0.0070381	0.0054765	0.0111121	0.0044596	5.9103582	0.0053043
133_VU109-K13_COMBINED	0.0253711	0.0002089	0.0404965	0.0003737	0.0081780	0.0052884	0.0139245	0.0034277	6.1053992	0.0039070
115_VU109-K13_COMBINED	0.0182973	0.0001745	0.0404741	0.0003309	0.0105403	0.0048820	0.0188356	0.0031360	4.1441850	0.0057389
134_VU109-K13_COMBINED	0.0253711	0.0002089	0.0404965	0.0003737	0.0081780	0.0052884	0.0139245	0.0034277	6.1053992	0.0039070
130_VU109-K13_COMBINED	0.0264190	0.0001451	0.0405574	0.0002356	0.0009214	0.0071580	0.0087545	0.0030740	6.2189960	0.0079885
131_VU109-K13_COMBINED	0.0264190	0.0001451	0.0405574	0.0002356	0.0009214	0.0071580	0.0087545	0.0030740	6.2189960	0.0079885
127_VU109-K13_COMBINED	0.0258794	0.0002401	0.0403968	0.0002192	0.0074780	0.0049684	0.0089134	0.0045211	6.1277551	0.0056314
118_VU109-K13_COMBINED	0.0306257	0.0001979	0.0400849	0.0002640	0.0027919	0.0027587	0.0170893	0.0042723	7.5075337	0.0067850

Sample Parameters	Material	Standard (Ma)	%1σ	J	%1σ	MDF	%1σ	Day	Time
119_VU109-K13_COMBINED	biotite	28.201	0.08	0.004673	0.19	0.994843	0.08	16.1.18	10:42
109_VU109-K13_COMBINED	biotite	28.201	0.08	0.004673	0.19	0.994843	0.08	16.1.18	5:06
124_VU109-K13_COMBINED	biotite	28.201	0.08	0.004673	0.19	0.994843	0.08	16.1.18	13:32
122_VU109-K13_COMBINED	biotite	28.201	0.08	0.004673	0.19	0.994843	0.08	16.1.18	12:25
116_VU109-K13_COMBINED	biotite	28.201	0.08	0.004673	0.19	0.994843	0.08	16.1.18	9:02
121_VU109-K13_COMBINED	biotite	28.201	0.08	0.004673	0.19	0.994843	0.08	16.1.18	11:49
128_VU109-K13_COMBINED	biotite	28.201	0.08	0.004673	0.19	0.994843	0.08	16.1.18	15:48
125_VU109-K13_COMBINED	biotite	28.201	0.08	0.004673	0.19	0.994843	0.08	16.1.18	14:05
133_VU109-K13_COMBINED	biotite	28.201	0.08	0.004673	0.19	0.994843	0.08	16.1.18	18:35
115_VU109-K13_COMBINED	biotite	28.201	0.08	0.004673	0.19	0.994843	0.08	16.1.18	8:26
134_VU109-K13_COMBINED	biotite	28.201	0.08	0.004673	0.19	0.994843	0.08	16.1.18	19:11
130_VU109-K13_COMBINED	biotite	28.201	0.08	0.004673	0.19	0.994843	0.08	16.1.18	16:55
131_VU109-K13_COMBINED	biotite	28.201	0.08	0.004673	0.19	0.994843	0.08	16.1.18	17:28
127_VU109-K13_COMBINED	biotite	28.201	0.08	0.004673	0.19	0.994843	0.08	16.1.18	15:12
118_VU109-K13_COMBINED	biotite	28.201	0.08	0.004673	0.19	0.994843	0.08	16.1.18	10:08

BE4 — K13 Single grain, size fraction 250–500 µm

Procedure Blanks	36Ar [fA]	1σ	37Ar [fA]	1σ	38Ar [fA]	1σ	39Ar [fA]	1σ	40Ar [fA]	1σ
039_VU109-K13	0.0478772	0.0003237	0.0765432	0.0045243	0.0041116	0.0031494	0.1155164	0.0031522	10.626874	0.013782
001_VU109-K13	0.0541900	0.0002673	0.0899850	0.0035863	0.0159668	0.0039784	0.1943091	0.0050960	10.712718	0.014668
033_VU109-K13	0.0505867	0.0001989	0.0680079	0.0067826	0.0009326	0.0035947	0.1248244	0.0034941	11.598251	0.015280
066_VU109-K13	0.0484664	0.0002378	0.0580562	0.0039179	0.0013215	0.0051341	0.1151794	0.0049921	11.385192	0.010425
015_VU109-K13	0.0514313	0.0003562	0.0752252	0.0046642	0.0076323	0.0044463	0.1478485	0.0045229	11.027274	0.009302
041_VU109-K13	0.0584922	0.0003335	0.0615235	0.0028569	0.0066797	0.0043523	0.1301354	0.0043251	14.167866	0.014239
035_VU109-K13	0.0453861	0.0002541	0.0615166	0.0041681	0.0028801	0.0043777	0.1327158	0.0042957	9.835250	0.009951
017_VU109-K13	0.0520155	0.0002553	0.0801819	0.0042241	0.0039091	0.0047428	0.1397380	0.0042463	11.426056	0.013755
021_VU109-K13	0.0625187	0.0003188	0.0630188	0.0033242	0.0022073	0.0041570	0.1365155	0.0048967	15.295315	0.010055
025_VU109-K13	0.0500169	0.0003443	0.0719787	0.0053075	0.0023167	0.0044591	0.1382881	0.0029722	11.111175	0.012854
027_VU109-K13	0.0500169	0.0003443	0.0719787	0.0053075	0.0023167	0.0044591	0.1382881	0.0029722	11.111175	0.012854
013_VU109-K13	0.0482869	0.0002195	0.0653062	0.0037402	0.0081687	0.0048047	0.1585921	0.0048568	9.761912	0.011737
019_VU109-K13	0.0563654	0.0003322	0.0575798	0.0047217	0.0107336	0.0051385	0.1403565	0.0052801	13.000625	0.012523
023_VU109-K13	0.0564459	0.0003106	0.0634203	0.0043960	0.0000542	0.0044401	0.1412385	0.0034370	13.105730	0.010265
064_VU109-K13	0.0445565	0.0002457	0.0631471	0.0047415	0.0014012	0.0040056	0.1193879	0.0044918	9.708129	0.016798
045_VU109-K13	0.0501933	0.0003137	0.0607942	0.0045010	0.0006490	0.0044099	0.1365732	0.0038386	11.404216	0.012266
043_VU109-K13	0.0476765	0.0002273	0.0642753	0.0038203	0.0008124	0.0030769	0.1328266	0.0033271	10.555891	0.006046
051_VU109-K13	0.0446798	0.0002889	0.0667025	0.0048285	0.0048772	0.0045999	0.1290127	0.0041770	9.809392	0.010484
049_VU109-K13	0.0469309	0.0002254	0.0569857	0.0033406	0.0059642	0.0052341	0.1156086	0.0027788	10.219745	0.014238
029_VU109-K13	0.0563848	0.0003394	0.0613804	0.0063180	0.0056471	0.0036200	0.1273151	0.0052820	13.246420	0.016881
047_VU109-K13	0.0586712	0.0003740	0.0424614	0.0047538	0.0059926	0.0037748	0.1245036	0.0035990	14.458831	0.014158
031_VU109-K13	0.0502347	0.0003046	0.0565894	0.0050099	0.0012747	0.0045605	0.1256198	0.0047793	11.238840	0.010577
062_VU109-K13	0.0442831	0.0001876	0.0549414	0.0046460	0.0066400	0.0046115	0.1189115	0.0043153	9.517689	0.011212
037_VU109-K13	0.0545840	0.0003478	0.0708174	0.0049347	0.0066918	0.0037842	0.1342910	0.0055207	12.936460	0.010794

Sample Parameters	Material	Standard (Ma)	%1σ	J	%1σ	MDF	%1σ	Day	Time
039_VU109-K13	biotite	28.201	0.08	0.004673	0.19	0.96387	0.02	27.9.17	4: 31
001_VU109-K13	biotite	28.201	0.08	0.004673	0.19	0.96387	0.02	26.9.17	16: 17
033_VU109-K13	biotite	28.201	0.08	0.004673	0.19	0.96387	0.02	27.9.17	2: 38
066_VU109-K13	biotite	28.201	0.08	0.004673	0.19	0.96387	0.02	27.9.17	13: 18
015_VU109-K13	biotite	28.201	0.08	0.004673	0.19	0.96387	0.02	26.9.17	21:01
041_VU109-K13	biotite	28.201	0.08	0.004673	0.19	0.96387	0.02	27.9.17	5:08
035_VU109-K13	biotite	28.201	0.08	0.004673	0.19	0.96387	0.02	27.9.17	3: 16
017_VU109-K13	biotite	28.201	0.08	0.004673	0.19	0.96387	0.02	26.9.17	21: 38
021_VU109-K13	biotite	28.201	0.08	0.004673	0.19	0.96387	0.02	26.9.17	22: 53
025_VU109-K13	biotite	28.201	0.08	0.004673	0.19	0.96387	0.02	27.9.17	0:08
027_VU109-K13	biotite	28.201	0.08	0.004673	0.19	0.96387	0.02	27.9.17	0: 46
013_VU109-K13	biotite	28.201	0.08	0.004673	0.19	0.96387	0.02	26.9.17	20: 23
019_VU109-K13	biotite	28.201	0.08	0.004673	0.19	0.96387	0.02	26.9.17	22: 16
023_VU109-K13	biotite	28.201	0.08	0.004673	0.19	0.96387	0.02	26.9.17	23: 31
064_VU109-K13	biotite	28.201	0.08	0.004673	0.19	0.96387	0.02	27.9.17	12: 41
045_VU109-K13	biotite	28.201	0.08	0.004673	0.19	0.96387	0.02	27.9.17	6: 23
043_VU109-K13	biotite	28.201	0.08	0.004673	0.19	0.96387	0.02	27.9.17	5: 45
051_VU109-K13	biotite	28.201	0.08	0.004673	0.19	0.96387	0.02	27.9.17	8: 15
049_VU109-K13	biotite	28.201	0.08	0.004673	0.19	0.96387	0.02	27.9.17	7: 38
029_VU109-K13	biotite	28.201	0.08	0.004673	0.19	0.96387	0.02	27.9.17	1: 23
047_VU109-K13	biotite	28.201	0.08	0.004673	0.19	0.96387	0.02	27.9.17	7:00
031_VU109-K13	biotite	28.201	0.08	0.004673	0.19	0.96387	0.02	27.9.17	2:01
062_VU109-K13	biotite	28.201	0.08	0.004673	0.19	0.96387	0.02	27.9.17	12:03
037_VU109-K13	biotite	28.201	0.08	0.004673	0.19	0.96387	0.02	27.9.17	3: 53

BE4 — K14 Single grain, size fraction 200–250 µm

Negative values in red

Procedure Blanks	36Ar [fA]	1σ	37Ar [fA]	1σ	38Ar [fA]	1σ	39Ar [fA]	1σ	40Ar [fA]	1σ
080_VU109-K14	0.0435015	0.0003030	0.0743106	0.0045531	0.0007966	0.0042853	0.1130284	0.0032350	9.466634	0.010624
090_VU109-K14	0.0528213	0.0002465	0.0769535	0.0041805	0.0005366	0.0051310	0.1133543	0.0051935	13.070540	0.009904
068_VU109-K14	0.0444235	0.0002095	0.0683006	0.0047305	0.0111377	0.0051705	0.1213968	0.0038926	10.027851	0.011019
119_VU109-K14	0.0609177	0.0002820	0.0677520	0.0039748	0.0089683	0.0043433	0.1033341	0.0051454	15.943547	0.014478
094_VU109-K14	0.0596425	0.0003873	0.0781944	0.0058036	0.0023741	0.0056267	0.1103117	0.0048862	15.303843	0.012194
125_VU109-K14	0.0601340	0.0003358	0.0705804	0.0028472	0.0070795	0.0031279	0.1071430	0.0028501	15.523696	0.011180
078_VU109-K14	0.0497660	0.0001785	0.0703752	0.0048665	0.0002167	0.0032317	0.1099610	0.0049200	11.702739	0.009703
098_VU109-K14	0.0471039	0.0002494	0.0633452	0.0042894	0.0062120	0.0053913	0.1182381	0.0020512	10.906837	0.008880
096_VU109-K14	0.0595492	0.0003753	0.0500912	0.0047955	0.0026333	0.0038961	0.1190773	0.0050305	15.234320	0.007165
123_VU109-K14	0.0446312	0.0003361	0.0501223	0.0066069	0.0000671	0.0039146	0.1097021	0.0036742	10.287024	0.008854
100_VU109-K14	0.0452926	0.0003299	0.0792860	0.0056167	0.0015161	0.0049523	0.1150500	0.0037065	10.182016	0.008290
074_VU109-K14	0.0464843	0.0003025	0.0638815	0.0060382	0.0039035	0.0044390	0.1109988	0.0051323	10.453414	0.013183
115_VU109-K14	0.0526085	0.0002746	0.0437497	0.0048233	0.0072559	0.0049292	0.1035638	0.0047615	13.143437	0.010540
092_VU109-K14	0.0467309	0.0003296	0.0550107	0.0058418	0.0006500	0.0044409	0.1134161	0.0033581	10.505972	0.014320
117_VU109-K14	0.0493684	0.0001925	0.0655509	0.0051994	0.0065897	0.0039987	0.1049400	0.0036206	11.833164	0.012995
072_VU109-K14	0.0759011	0.0002995	0.0692429	0.0041446	0.0049697	0.0043791	0.1050943	0.0054208	20.766550	0.017121
084_VU109-K14	0.0541932	0.0002791	0.0639174	0.0023461	0.0014787	0.0056946	0.1141352	0.0052650	13.123859	0.011187
086_VU109-K14	0.0488497	0.0002001	0.0532027	0.0063060	0.0022094	0.0039221	0.1161357	0.0046957	11.388452	0.012683
082_VU109-K14	0.1152449	0.0003591	0.0613211	0.0055907	0.0087317	0.0047049	0.1156490	0.0045586	33.877301	0.010565
121_VU109-K14	0.0519553	0.0003288	0.0609775	0.0051079	0.0048773	0.0049873	0.1028078	0.0036119	12.758032	0.009665
070_VU109-K14	0.0464068	0.0002161	0.0622649	0.0045734	0.0024187	0.0045147	0.1159880	0.0059010	10.581207	0.006487
088_VU109-K14	0.0518799	0.0004092	0.0539732	0.0050925	0.0002552	0.0051398	0.1191722	0.0046253	12.519998	0.014122
076_VU109-K14	0.0468017	0.0002686	0.0663884	0.0053969	0.0076638	0.0027794	0.1118769	0.0042247	10.814624	0.011085
113_VU109-K14	0.0506757	0.0002856	0.0575892	0.0059643	0.0015275	0.0030536	0.1061590	0.0037504	12.152172	0.010687
111_VU109-K14	0.0725248	0.0003058	0.0654755	0.0047109	0.0114764	0.0048502	0.1134391	0.0045535	19.985227	0.015123

Sample Parameters	Material	Standard (Ma)	%1σ	J	%1σ	MDF	%1σ	Day	Time
080_VU109-K14	biotite	28.201	0.08	0.00468	0.03	0.96387	0.02	27.9.17	17:40
090_VU109-K14	biotite	28.201	0.08	0.00468	0.03	0.96387	0.02	27.9.17	20:48
068_VU109-K14	biotite	28.201	0.08	0.00468	0.03	0.96387	0.02	27.9.17	13:56
119_VU109-K14	biotite	28.201	0.08	0.00468	0.03	0.96387	0.02	28.9.17	6:13
094_VU109-K14	biotite	28.201	0.08	0.00468	0.03	0.96387	0.02	27.9.17	22:03
125_VU109-K14	biotite	28.201	0.08	0.00468	0.03	0.96387	0.02	28.9.17	8:05
078_VU109-K14	biotite	28.201	0.08	0.00468	0.03	0.96387	0.02	27.9.17	17:03
098_VU109-K14	biotite	28.201	0.08	0.00468	0.03	0.96387	0.02	27.9.17	23:18
096_VU109-K14	biotite	28.201	0.08	0.00468	0.03	0.96387	0.02	27.9.17	22:40
123_VU109-K14	biotite	28.201	0.08	0.00468	0.03	0.96387	0.02	28.9.17	7: 28
100_VU109-K14	biotite	28.201	0.08	0.00468	0.03	0.96387	0.02	27.9.17	23:55
074_VU109-K14	biotite	28.201	0.08	0.00468	0.03	0.96387	0.02	27.9.17	15: 48
115_VU109-K14	biotite	28.201	0.08	0.00468	0.03	0.96387	0.02	28.9.17	4:58
092_VU109-K14	biotite	28.201	0.08	0.00468	0.03	0.96387	0.02	27.9.17	21:25
117_VU109-K14	biotite	28.201	0.08	0.00468	0.03	0.96387	0.02	28.9.17	5:35
072_VU109-K14	biotite	28.201	0.08	0.00468	0.03	0.96387	0.02	27.9.17	15:11
084_VU109-K14	biotite	28.201	0.08	0.00468	0.03	0.96387	0.02	27.9.17	18:55
086_VU109-K14	biotite	28.201	0.08	0.00468	0.03	0.96387	0.02	27.9.17	19: 33
082_VU109-K14	biotite	28.201	0.08	0.00468	0.03	0.96387	0.02	27.9.17	18:18
121_VU109-K14	biotite	28.201	0.08	0.00468	0.03	0.96387	0.02	28.9.17	6:50
070_VU109-K14	biotite	28.201	0.08	0.00468	0.03	0.96387	0.02	27.9.17	14:33
088_VU109-K14	biotite	28.201	0.08	0.00468	0.03	0.96387	0.02	27.9.17	20:10
076_VU109-K14	biotite	28.201	0.08	0.00468	0.03	0.96387	0.02	27.9.17	16:25
113_VU109-K14	biotite	28.201	0.08	0.00468	0.03	0.96387	0.02	28.9.17	4:20
111_VU109-K14	biotite	28.201	0.08	0.00468	0.03	0.96387	0.02	28.9.17	3:43

Information on Analysis and used Constants for all samples of BE4 (K13, K13b, K14)	
Analysis	
Material	biotite
Location	Berhardstal 4 well
Analyst	K. Kuiper
Project	VU109
Mass Discr. Law	LIN
Irradiation	VU109
J (K13, K13b)	0.00467330 ± 0.00000888
J (K14)	0.00467960 ± 0.00000140
FCs	28.201 ± 0.023 Ma
Heating	45 sec
Isolation	3.00 min
Instrument	ARGUS
Constants	
Age Equations	Min et al. (2000)
Negative Intensities	Allowed
Decay Constant 40K	5.460 ± 0.053 E-10 1/a
Decay Constant 39Ar	2.940 ± 0.016 E-07 1/h
Decay Constant 37Ar	8.230 ± 0.012 E-04 1/h
Decay Constant 36Cl	2.257 ± 0.015 E-06 1/a
Decay Activity 40K(EC,β^+)	3.310 ± 0.030 1/gs
Decay Activity 40K(β^-)	27.890 ± 0.150 1/gs
Atmospheric Ratio 40/36(a)	298.56 ± 0.31
Atmospheric Ratio 38/36(a)	0.1885 ± 0.0003
Production Ratio 39/37(ca)	0.000673 ± 0.000004
Production Ratio 36/37(ca)	0.000264 ± 0.000002
Production Ratio 40/39(k)	0.000860 ± 0.000070
Production Ratio 38/39(k)	0.012110 ± 0.000030
Production Ratio 36/38(cl)	262.80 ± 1.71
Scaling Ratio K/Ca	0.43
Abundance Ratio 40K/K	1.1700 ± 0.0100 E-04
Atomic Weight K	39.0983 ± 0.0001 g

C) KH2: Kamenica nad Hronom, Danube Basin

Sample KH2 — code K15: hornblende

Age result KH2 (hornblende)	40(a)/36(a)	± 2σ	40(r)/39(k)	± 2σ	Age (Ma)	± 2σ	MSWD	N	K/Ca	± 2σ
Weighted mean age			1.47268	± 0.00987	12.56	± 0.10	1.27	58.10	0.086	± 0.004
				± 0.67 %		± 0.77 %	25 %	10		
					External Error	± 0.28	1.94	2σ Confidence Limit		
					Analytical Error	± 0.08	1.1281	*Error Magnification*		
Normal Isochron	298.73	± 2.61	1.47114	± 0.01904	12.55	± 0.17	1.44	58.10		
		± 0.87%		± 1.29 %		± 1.34 %	17 %	10		
					External Error	± 0.31	2.00	2σ Confidence Limit		
					Analytical Error	± 0.16	1.1992	*Error Magnification*		
						17		*Number of Iterations*		
						0.0000108201		*Convergence*		
Inverse Isochron	298.69	± 2.62	1.47189	± 0.01908	12.56	± 0.17	1.45	58.10		
		± 0.88%		± 1.30 %		± 1.35 %	17 %	10		
					External Error	± 0.31	2.00	2σ Confidence Limit		
					Analytical Error	± 0.16	1.2057	*Error Magnification*		
							3	*Number of Iterations*		
							0.0002975403	*Convergence*		
							42 %	*Spreading Factor*		

KH2 (K15) hornblende

Relative abundances	Selected for mean age calc.	36Ar [fA]	%1σ	37Ar [fA]	%1σ	38Ar [fA]	%1σ	39Ar [fA]	%1σ	40Ar [fA]	%1σ	40(r)/39 (k)	± 2σ	Age	± 2σ	40Ar(r)	39Ar(k)	K/Ca	± 2σ
144_VU109-K15		0.3209394	0.384	38.8537	1.302	0.323798	2.201	7.19880	0.115	102.9944	0.015	1.43033	± 0.10683	12.20	± 0.91	9.96	2.23	0.079	± 0.002
152_VU109-K15		0.0942808	0.637	22.4515	1.505	0.149898	5.504	4.23981	0.182	32.4752	0.088	1.44524	± 0.08823	12.33	± 0.75	18.80	1.31	0.081	± 0.002
146_VU109-K15		0.6216748	0.366	55.1470	1.130	0.463482	1.270	9.93377	0.098	195.5654	0.011	1.44823	± 0.14287	12.35	± 1.21	7.33	3.07	0.077	± 0.002
159_VU109-K15	x	0.1514981	0.444	158.9143	1.067	1.107321	0.514	30.50546	0.105	76.8934	0.140	1.45651	± 0.01856	12.42	± 0.16	57.58	9.44	0.082	± 0.002
168_VU109-K15	x	0.2571300	0.441	156.0166	1.152	1.082511	0.577	30.44966	0.103	108.6568	0.156	1.45878	± 0.02767	12.44	± 0.24	40.74	9.43	0.084	± 0.002
149_VU109-K15	x	0.1326654	0.503	36.1011	1.276	0.332333	2.691	9.07113	0.113	49.9466	0.044	1.45989	± 0.04612	12.45	± 0.39	26.44	2.81	0.108	± 0.003
165_VU109-K15	x	0.2754689	0.445	158.3879	1.056	1.112311	0.527	31.48667	0.103	115.5092	0.097	1.46053	± 0.02688	12.46	± 0.23	39.68	9.75	0.085	± 0.002
164_VU109-K15	x	0.2402838	0.411	104.9198	1.143	0.692800	0.841	20.31357	0.089	93.2655	0.067	1.47426	± 0.03241	12.58	± 0.28	32.00	6.29	0.083	± 0.002
150_VU109-K15	x	0.0963715	0.605	74.8484	1.116	0.489844	1.577	14.53197	0.088	44.2711	0.092	1.48002	± 0.02715	12.62	± 0.23	48.41	4.50	0.083	± 0.002
162_VU109-K15	x	0.0977445	0.548	108.8273	1.079	0.808060	0.991	23.08184	0.100	54.6977	0.118	1.48445	± 0.01801	12.66	± 0.15	62.44	7.15	0.091	± 0.002
137_VU109-K15	x	0.1588356	0.473	44.0200	1.077	0.318504	2.055	8.90108	0.098	57.1014	0.031	1.48659	± 0.05316	12.68	± 0.45	23.07	2.75	0.087	± 0.002
156_VU109-K15	x	0.2564404	0.404	61.2766	1.231	0.462875	1.291	12.05784	0.094	89.6591	0.059	1.49451	± 0.05491	12.75	± 0.47	20.03	3.73	0.084	± 0.002
147_VU109-K15	x	0.0400736	0.896	38.5093	1.373	0.273992	2.697	7.28016	0.108	19.8083	0.093	1.50280	± 0.03284	12.82	± 0.28	55.04	2.25	0.081	± 0.002
167_VU109-K15		0.2125266	0.443	157.4749	1.022	1.058578	0.789	30.53571	0.085	97.1038	0.052	1.51636	± 0.02164	12.93	± 0.18	47.52	9.45	0.083	± 0.002
143_VU109-K15		0.1136601	0.466	69.0686	1.099	0.466515	1.376	13.70696	0.099	49.3308	0.026	1.52802	± 0.02590	13.03	± 0.22	42.31	4.24	0.085	± 0.002
161_VU109-K15		0.1231536	0.577	113.4949	1.094	0.737675	1.409	23.19828	0.092	63.4748	0.069	1.54406	± 0.02148	13.17	± 0.18	56.25	7.18	0.088	± 0.002
155_VU109-K15		0.1458331	0.607	78.7183	1.226	0.554937	1.218	16.71963	0.089	63.1047	0.049	1.54844	± 0.03399	13.21	± 0.29	40.90	5.18	0.091	± 0.002
158_VU109-K15		0.1316138	0.549	92.3778	1.047	0.604064	1.225	21.34394	0.088	64.9489	0.073	1.54916	± 0.02277	13.21	± 0.19	50.76	6.61	0.099	± 0.002
153_VU109-K15		0.4798517	0.370	43.5926	1.181	0.350903	2.154	8.46717	0.109	153.2053	0.020	1.58748	± 0.13113	13.54	± 1.11	8.74	2.62	0.083	± 0.002
	Σ	**3.9500457**	**0.114**	**1613.0005**	**0.286**	**11.390402**	**0.279**	**323.02344**	**0.025**	**1532.0123**	**0.018**								

KH2 (K15) hornblende

Negative values in red

Procedure Blanks	36Ar [fA]	1σ	37Ar [fA]	1σ	38Ar [fA]	1σ	39Ar [fA]	1σ	40Ar [fA]	1σ
144_VU109-K15	0.0248431	0.0002015	0.0418771	0.0001767	0.0086171	0.0040510	0.0009624	0.0031554	5.7908576	0.0090525
152_VU109-K15	0.0280143	0.0001049	0.0427599	0.0002551	0.0029772	0.0047958	0.0119261	0.0038482	6.6019619	0.0206998
146_VU109-K15	0.0268093	0.0002273	0.0424771	0.0003098	0.0035991	0.0044700	0.0131411	0.0036590	6.2654033	0.0132104
159_VU109-K15	0.0303463	0.0001593	0.0429715	0.0003111	0.0013323	0.0043634	0.0155571	0.0025791	7.2672913	0.0107135
168_VU109-K15	0.0377447	0.0002077	0.0461329	0.0006425	0.0165510	0.0051228	0.0416512	0.0026376	9.6296780	0.0222595
149_VU109-K15	0.0273030	0.0003026	0.0424297	0.0002702	0.0101628	0.0066015	0.0065075	0.0031731	6.3789952	0.0139366
165_VU109-K15	0.0346295	0.0003230	0.0453123	0.0004012	0.0149117	0.0029313	0.0404516	0.0038749	8.8377453	0.0139817
164_VU109-K15	0.0346295	0.0003230	0.0453123	0.0004012	0.0149117	0.0029313	0.0404516	0.0038749	8.8377453	0.0139817
150_VU109-K15	0.0273030	0.0003026	0.0424297	0.0002702	0.0101628	0.0066015	0.0065075	0.0031731	6.3789952	0.0139366
162_VU109-K15	0.0343109	0.0003435	0.0444778	0.0003891	0.0219103	0.0059228	0.0414773	0.0027075	8.5543665	0.0140600
137_VU109-K15	0.0255663	0.0002418	0.0410773	0.0001794	0.0059036	0.0051091	0.0047054	0.0033897	6.0527293	0.0067506
156_VU109-K15	0.0284756	0.0002437	0.0428328	0.0002594	0.0132784	0.0041307	0.0111049	0.0037732	6.6399978	0.0203133
147_VU109-K15	0.0268093	0.0002273	0.0424771	0.0003098	0.0035991	0.0044700	0.0131411	0.0036590	6.2654033	0.0132104
167_VU109-K15	0.0377447	0.0002077	0.0461329	0.0006425	0.0165510	0.0051228	0.0416512	0.0026376	9.6296780	0.0222595
143_VU109-K15	0.0248431	0.0002015	0.0418771	0.0001767	0.0086171	0.0040510	0.0009624	0.0031554	5.7908576	0.0090525
161_VU109-K15	0.0343109	0.0003435	0.0444778	0.0003891	0.0219103	0.0059228	0.0414773	0.0027075	8.5543665	0.0140600
155_VU109-K15	0.0284756	0.0002437	0.0428328	0.0002594	0.0132784	0.0041307	0.0111049	0.0037732	6.6399978	0.0203133
158_VU109-K15	0.0303463	0.0001593	0.0429715	0.0003111	0.0013323	0.0043634	0.0155571	0.0025791	7.2672913	0.0107135
153_VU109-K15	0.0280143	0.0001049	0.0427599	0.0002551	0.0029772	0.0047958	0.0119261	0.0038482	6.6019619	0.0206998

Sample Parameters	Material	Standard (Ma)	%1σ	J	%1σ	MDF	%1σ	Day	Time
144_VU109-K15	hornblende	28.201	0.08	0.004673	0.19	0.994843	0.08	17.1.18	0:47
152_VU109-K15	hornblende	28.201	0.08	0.004673	0.19	0.994843	0.08	17.1.18	5:17
146_VU109-K15	hornblende	28.201	0.08	0.004673	0.19	0.994843	0.08	17.1.18	1:54
159_VU109-K15	hornblende	28.201	0.08	0.004673	0.19	0.994843	0.08	17.1.18	9:13
168_VU109-K15	hornblende	28.201	0.08	0.004673	0.19	0.994843	0.08	17.1.18	14:19
149_VU109-K15	hornblende	28.201	0.08	0.004673	0.19	0.994843	0.08	17.1.18	3:34
165_VU109-K15	hornblende	28.201	0.08	0.004673	0.19	0.994843	0.08	17.1.18	12:36
164_VU109-K15	hornblende	28.201	0.08	0.004673	0.19	0.994843	0.08	17.1.18	12:03
150_VU109-K15	hornblende	28.201	0.08	0.004673	0.19	0.994843	0.08	17.1.18	4:10
162_VU109-K15	hornblende	28.201	0.08	0.004673	0.19	0.994843	0.08	17.1.18	10:56
137_VU109-K15	hornblende	28.201	0.08	0.00468	0.03	0.994843	0.08	16.1.18	20:51
156_VU109-K15	hornblende	28.201	0.08	0.004673	0.19	0.994843	0.08	17.1.18	7:33
147_VU109-K15	hornblende	28.201	0.08	0.004673	0.19	0.994843	0.08	17.1.18	2:27
167_VU109-K15	hornblende	28.201	0.08	0.004673	0.19	0.994843	0.08	17.1.18	13:43
143_VU109-K15	hornblende	28.201	0.08	0.004673	0.19	0.994843	0.08	17.1.18	0:11
161_VU109-K15	hornblende	28.201	0.08	0.004673	0.19	0.994843	0.08	17.1.18	10:20
155_VU109-K15	hornblende	28.201	0.08	0.004673	0.19	0.994843	0.08	17.1.18	6:57
158_VU109-K15	hornblende	28.201	0.08	0.004673	0.19	0.994843	0.08	17.1.18	8:40
153_VU109-K15	hornblende	28.201	0.08	0.004673	0.19	0.994843	0.08	17.1.18	5:50

Information on Analysis and used Constants for all samples of KH2	
Analysis	
Material	hornblende
Location	Kamenice nad Hronom village - quarry
Analyst	K. Kuiper
Project	VU109
Mass Discr. Law	LIN
Irradiation	VU109
J (K13, K13b)	0.00467330 ± 0.00000888
FCs	28.201 ± 0.023 Ma
Heating	45 sec
Isolation	3.00 min
Instrument	ARGUS
Constants	
Age Equations	Min et al. (2000)
Negative Intensities	Allowed
Decay Constant 40K	5.460 ± 0.053 E-10 1/a
Decay Constant 39Ar	2.940 ± 0.016 E-07 1/h
Decay Constant 37Ar	8.230 ± 0.012 E-04 1/h
Decay Constant 36Cl	2.257 ± 0.015 E-06 1/a
Decay Activity 40K(EC,β^+)	3.310 ± 0.030 1/gs
Decay Activity 40K(β^-)	27.890 ± 0.150 1/gs
Atmospheric Ratio 40/36(a)	298.56 ± 0.31
Atmospheric Ratio 38/36(a)	0.1885 ± 0.0003
Production Ratio 39/37(ca)	0.000673 ± 0.000004
Production Ratio 36/37(ca)	0.000264 ± 0.000002
Production Ratio 40/39(k)	0.000860 ± 0.000070
Production Ratio 38/39(k)	0.012110 ± 0.000030
Production Ratio 36/38(cl)	262.80 ± 1.71
Scaling Ratio K/Ca	0.43
Abundance Ratio 40K/K	1.1700 ± 0.0100 E-04
Atomic Weight K	39.0983 ± 0.0001 g